New Immobilized Antimicrobial Polyethylenimines: Synthesis and Properties

by

Harris K. Liu

B.S. Chemistry and Biochemistry
University of California, Santa Barbara, 2010

SUBMITTED TO THE DEPARTMENT OF CHEMISTRY IN PARTIAL FULFILLMENT OF THE REQUIREMENTS FOR THE DEGREE OF

MASTER OF SCIENCE IN CHEMISTRY
AT THE
MASSACHUSETTS INSTITUTE OF TECHNOLOGY

SEPTEMBER 2014

Signature of Author: Signature redacted

Department of Chemistry
August 22, 2014

Certified by: Signature redacted

Alexander M. Klibanov
Novartis Professor of Chemistry and Bioengineering

Accepted by: Signature redacted

Robert W. Field
Chairman, Departmental Committee on Graduate Students

New Immobilized Antimicrobial Polyethylenimines: Synthesis and Properties

by

Harris K. Liu

Submitted to the Department of Chemistry
on August 22nd, 2014 in Partial Fulfillment of the
Requirements for the Degree of

Master of Science in Chemistry

ABSTRACT

Surfaces modified with immobilized *N*-alkyl-polyethylenimines (*N*-alkyl-PEIs) containing various alkyl groups were synthesized and tested against various pathogenic human influenza viruses to establish structure-to-virucidal activity relationships. Various physical-chemical properties of each surface were correlated with their virucidal activities to identify key antiviral surface properties. The accessibility of *N*-alkyl-PEI quaternary ammonium groups to influenza virus was subsequently identified as the key determinant of antiviral efficacy, as demonstrated by FITC-lysozyme surface titration.

Previously used multistep syntheses to create antimicrobial surfaces by immobilizing *N*-alkyl-PEIs were replaced with a novel aerosol-assisted plasma deposition procedure. *N,N*-hexyl,methyl-polyethylenimines were directly plasma-coated onto a glass surface. The resulting material was thoroughly characterized and demonstrated to be robust, scalable, bactericidal against *Escherichia coli*, and virucidal against human influenza virus.

Biocompatibility and bactericidal properties of *N*-alkyl-PEIs immobilized on Boston Keratoprosthetic implants were evaluated *in vivo*. Surface-attached *N,N*-hexyl,methyl-polyethylenimines exhibited inhibitory effects on *Staphylococcus aureus* biofilm formation, with no toxicity or adverse reactivity detected.

Thesis Supervisor: Alexander M. Klibanov

Title: Novartis Professor of Chemistry and Bioengineering

Introduction

Infectious diseases annually affect more than two billion people and kill over 12 million.[1] The vast majority of infectious diseases are caused by bacteria or viruses and are prevalent in both developing and developed countries. Many microbial pathogens are disseminated by fomites, generally involving deposition of a microbe onto the surface of an object and its subsequent transfer to an individual who contacts the contaminated region.[2,3] Current measures to prevent the spread of communicable diseases predominantly utilize drugs, such as antibiotics for bacteria or antiviral medications for viruses, which target either the corresponding pathogens or their associated host biochemical pathways *in vivo*.[4] However, the evolution of drug-resistant strains of bacteria and viruses has decreased the efficiency of these drugs in countering infections.[5,6] Thus, new approaches to limiting the spread of infectious diseases, such as by creating pathogen-inactivating surfaces, should be explored.[7]

Numerous methods have been developed to generate surfaces that disinfect pathogens. These approaches commonly involve impregnating porous materials with antimicrobial compounds which slowly release over time.[8,9] Such designs are consequently temporary and result in contamination of their surrounding environments with biocides. Therefore, elaborating more permanent antimicrobial surfaces is desirable.[7]

Several surface modifications, such as covalently-attached cationic polymers, have so far been demonstrated to kill bacteria and viruses.[10,11,12,13] Among these, *N*-alkyl-polyethylenimines (*N*-alkyl-PEIs) have shown very high antimicrobial activities against Gram-positive and Gram-negative bacteria, fungi, and influenza viruses.[14,15] Prior studies have explored the mechanisms by which *Escherichia coli*, *Staphylococcus aureus*, and human influenza A viruses are

inactivated by immobilized *N*-alkyl-PEIs and have tested various methods of applying the polymers to surfaces.[16]

While the ability of *N*-alkyl-PEIs to eliminate influenza is established, it is still unknown what specific surface property or molecular component is responsible for observed virucidal activity. The main portion of this thesis work thus attempts to elucidate structure-activity relationships (SARs) between surfaces-immobilized *N*-alkyl-PEIs and their anti-influenza virucidal activities. In addition, novel methods of immobilizing *N*-alkyl-PEIs, along with *in vivo* testing of the immobilized polymers as a corneal prosthetic model, are described herein.

References

1. World Health Organization - World Health Statistics 2014; 20 August 2014. Available from: **http://www.who.int/gho/publications/world_health_statistics/EN_WHS2014_Part3.pdf**
2. Haas, C.N.; Rose, J.B.; Gerba, C.P. In *Quantitative Microbial Risk Assessment*; Haas, C.N., Rose, J.B., Gerba, C.P., Eds.; J. Wiley and Sons, Inc: New York, NY, 1999; p.35-50
3. Boone, S.A.; Gerba, C.P. *Appl. Environ. Microbiol.* **2007**, *73*, 1687-1696
4. Lewis, K. *Annu. Rev. Microbiol.* **2010**, *64*, 357-372
5. Pray, L. *Nature Education* **2008**, *1*, 30-33
6. Liang, Z.; Li, L.; Wang, Y.; Jiang, H. *PloS One* **2011**, *6*, 1-8
7. Klibanov, A.M. *J. Mater. Chem.* **2007**, *17*, 2479-2482
8. Gao, P.; Nie, X.; Zou, M.; Shi, Y.; Cheng, G. *J. Antibiot.* **2011**, *64*, 625-634
9. Jung, W.K.; Koo, H.C.; Kim, K.W.; Shin, S.; Kim, S.H.; Park, Y.H. *Appl. Environ. Microbiol.* **2008**, *74*, 2171-2178
10. Tiller, J.C.; Liao, C.J.; Lewis, K.; Klibanov, A.M. *Proc. Natl. Acad. Sci. U.S.A.* **2001**, *98*, 5981-5985
11. Mukherjee, K.; Rivera, J.J.; Klibanov, A.M. *Appl. Biochem. Biotechnol.* **2008**, *151*, 61-70
12. Timofeeva, L.; Kleshcheva, N. *Appl. Microbiol. Biotechnol.* **2011**, *89*, 475-492
13. Cowan, M.M.; Abshire, K.Z.; Houk, S.L.; Evans, S.M. *J. Ind. Miocrobiol. Biotechnol.* **2003**, *30*, 102-106
14. Lin, J.; Qiu, S.; Lewis, K.; Klibanov, A.M. *Biotechnol. Bioeng.* **2003**, *83*, 168-172
15. Haldar, J.; An, D.; de Cienfuegos, L.A.; Chen, J.; Klibanov, A.M. *Proc. Natl. Acad. Sci. U.S.A.* **2006**, *103*, 17667-17671
16. Hsu, B.B.; Wong, S.Y.; Hammond, P.T.; Chen, J.; Klibanov, A.M. *Proc. Natl. Acad. Sci. U.S.A.* **2011**, *108*, 61-66

Why do some immobilized *N*-alkyl-polyethylenimines far surpass others in inactivating influenza viruses?

Introduction

Influenza (flu) viruses pose a global health threat. They infect 5 to 15% of worldwide human population annually, and kill millions of people.[1] Because influenza viruses propagate rapidly in populations and are commonly spread via fomites, developing surfaces that strongly debilitate influenza is critical.[2] Several types of antimicrobial surface coatings currently exist,[3,4,5] of which only a few have been demonstrated to kill influenza viruses. Among these, immobilized (covalently-attached) or painted *N*-alkyl-polyethylenimines (*N*-alkyl-PEIs) were developed and shown to inactivate the viruses.[6,7,8] Previous experiments have attempted to understand the mechanism of influenza killing by these surfaces.[9] However, whether a specific molecular determinant or surface property is responsible for virucidal activity of *N*-alkyl-PEI surfaces remains unclear.

In the present study, we have attempted to establish structure-activity relationships between surfaces modified with immobilized *N*-alkyl-PEIs and their virucidal activities. To this end, we synthesized *N*-alkyl-polyethylenimines with various alkyl functional groups and determined their antiviral activities towards various influenza strains (H1N1 PR8, H3N2 Wuhan, WSN). Several physical-chemical properties of each surface were measured, including contact angle, surface charge, quaternary ammonium group density, and surface roughness, then correlated with surface antiviral activities to identify significant causes of antiviral activity. Results showed only one good correlation, revealing virucidal activity to be dependent on the accessibility of quaternary ammonium groups to a macromolecular entity (and thus influenza virus). Based on the experiments detailed herein, we conclude that the accessibility of quaternary

ammonium groups to influenza viruses is the primary determinant of immobilized *N*-alkyl-PEI surface virucidal activity.

Materials and Methods

Materials.

All chemicals were acquired from Sigma-Aldrich and used as received unless otherwise noted. Glass slides (75 × 25 × 1 mm) from Corning, and polypropylene sheets (12" × 12" × 1/16") from McMaster-Carr were cut into square (25 × 25 × 1 mm) pieces. Madin-Darby canine kidney cells were procured from the American Type Culture Collection (Manassas, VA). Influenza A/PR/8/34 (H1N1), influenza A/WSN/33 (H1N1), and influenza A/Wuhan/359/95 (H3N2) viruses were cultured from MDCK cells and stored at -80°C prior to use.

Immobilized *N*-alkyl-polyethylenimine Synthesis.

Linear, 200-kDa polyethylenimine (PEI) was prepared by hydrolyzing commercial 500-kDa poly(2-ethyl-2-oxazoline) as detailed previously.[10] Clean glass slides were placed in a solution of 10% (3-aminopropyl)triethoxysilane in toluene and refluxed for 2 h (see **Scheme 1**). After rinsing with chloroform, aminated-slides were acylated in a solution of 10 mL of 4-bromobutyryl chloride and 90 mL of chloroform for 6 h stirring at room temperature. Resultant slides were air-dried. rinsed with *tert*-amyl alcohol, and placed in 90 mL of *tert*-amyl alcohol with 10 g of linear PEI and 2 g of K_2CO_3. The reaction was stirred for 12 h at 95°C to yield PEI slides. The PEI-attached slides were then *N*-alkylated by addition of 30 mL of a primary linear bromoalkane in 70 mL of *tert*-amyl alcohol at 95°C for 12 h to generate *N*-alkyl-PEI slides. Subsequent treatment of *N*-alkyl-PEI slides with 20 mL of iodomethane in 80 mL of *tert*-amyl alcohol at 60°C for 9 h produced *N,N*-alkyl,methyl-PEI slides. Permethyl-PEI-attached slides

were synthesized by placing PEI-modified slides into 20 mL of iodomethane and 80 mL of *tert*-amyl alcohol at 60°C for 9 h.

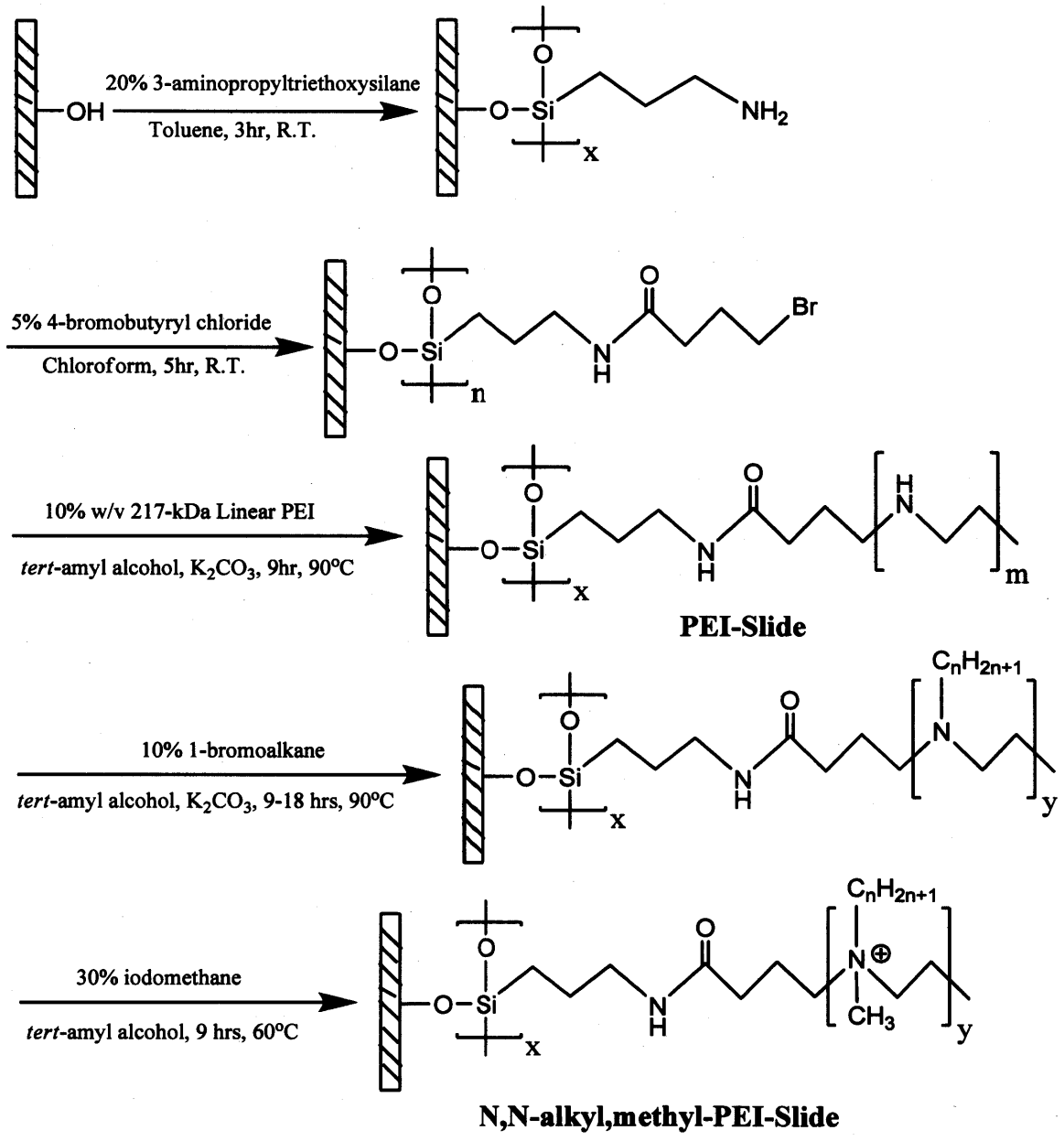

Scheme 1. Synthesis of immobilized *N*-alkyl-polyethylenimines

FITC/RITC-Lysozyme Synthesis.

Fluorescein isothiocyanate and rhodamine-B isothiocyanate were attached to lysozyme, yielding FITC-Lys and RITC-Lys, respectively, as detailed in prior literature.[11,12] Conjugates were purified by dialyzing three times for 12 h each at 4°C in 10 kDa molecular-weight cut-off dialysis bags in 0.01 M phosphate buffer, pH 8.1. The solution was passed through a CM Sephadex C-25 column (3 × 25 cm), and the second pigmented fraction collected. Dye to protein ratios were then determined by spectrophotometer.

Contact Angle.

Contact angles of each *N*-alkyl-PEI surface were measured with a Ramé-Hart 590 goniometer using the sessile drop method. Contact angle measurements were taken in triplicate for six different areas on each sample with ~5μL of de-ionized water and averaged.

Surface Zeta Potential.

Surface zeta potentials of each *N*-alkyl-PEI surface were determined using a flat surface cell with a Beckman Coulter DelsaNano C instrument. Runs were performed in triplicate using stock standard nanoparticles in 10mM NaCl at room temperature.

Quaternary Ammonium Group Density Determination and FITC/RITC/Native-Lysozyme Adsorption.

Fluorescein was used to determine the quaternary ammonium group density as previously described.[13] Each *N*-alkyl-PEI slide was shaken for 15 min in a 1% *w/v* fluorescein Na salt in phosphate-buffered solution (PBS, 0.1 M NaH_2PO_4, pH 8.0), rinsed thrice with dye-free buffer, then agitated in 45 mL of 0.1% *w/v* cetyltrimethylammonium chloride for 15 min to desorb the

dye. The quaternary ammonium group density of each sample was determined by observing the absorbance of the resultant solution at 501 nm and using the previously measured fluorescein extinction coefficient of 77 $mM^{-1}cm^{-1}$. The same procedure was used to analyze FITC-Lys and adsorption to *N*-alkyl-PEI slides, using a 5 mg/mL solution of FITC-Lys instead of fluorescein. RITC-Lys adsorption was determined similarly, with the exception of measuring absorbance at 555 nm.

Native lysozyme adsorption onto *N*-alkyl-PEI slides was determined as follows: Sample slides were placed in 45 mL of 50 mg/mL lysozyme in PBS, shaken for 15 min, rinsed with buffer, then agitated in 0.01% *w/v* Tween 20. The amount of desorbed protein in solution was then determined by Bradford assay (Bio-Rad Quick Start™ Bradford).

Atomic Force Microscopy.

Surface roughness, adhesive interactions (contact force mode), and polymer chain extension lengths were measured by atomic force microscopy (AFM). An SCM-PIT AFM probe tip (Pt-Ir coated, nominal spring constant 2.8 N/m, Bruker, Camarillo, CA) was used in tapping mode on a Dimension 3100 scanner (Veeco, Santa Barbara, CA) to measure ambient-condition surface roughnesses of each *N*-alkyl-PEI slide over 0.25 μm^2 sample areas. Six representative regions were sampled for each slide. Roughness parameters calculated were arithmetic average (Ra), root-mean squared average (Rrms), and maximum peak-valley distances (Z-range).

Contact force and polymer chain extension measurements were performed with sharpened silicon-nitride probe tips (ORC8-10, nominal spring constant 0.11 N/m, Bruker, Camarillo, CA) in contact mode in PBS (pH 8.0) at room temperature. Contact force was then calculated from the measured deflection, deflection sensitivity of the probe, and spring constant.

Polymer chain extension lengths were derived from force curve points corresponding to initial probe tip attachment to the surface and subsequent probe tip detachment.[14]

Determination of Virucidal Activities.

Virucidal activities of each *N*-alkyl-PEI slide were determined by methods described in previous literature.[15] 10 μL of influenza virus (WSN, PR8, or Wuhan) at a concentration of ~10^8 plaque forming units (PFU)/mL was added to the center or a treated slide. The droplet was then covered and spread with a polypropylene slide. Virus-exposed sides of both slides were subsequently washed with 990 μL of PBS after incubating for 10 minutes. PBS was used for twofold serial dilutions of each washing, and 200 μL of each dilution was added to confluent Madin-Darby canine kidney cells in six-well tissue culture plates to quantify plaques, and thus, viral titer.

Results and Discussion

Virucidal activities for painted *N*-alkyl-PEIs were determined in prior experiments, and demonstrated that certain PEIs have higher virus-inactivating abilities than others.[6] However, the specific molecular entity or surface property which influenced viral-inactivation remained unknown. In addition, anti-influenza efficacy has never previously been demonstrated with permanently immobilized (covalently-attached) *N*-alkyl-PEIs. Hsu, *et al.* showed loss of viral proteins and infectivity when painted *N*-alkyl-PEIs were exposed to viral solutions.[9] Meanwhile, tangentially-related experiments with bacteria indicated antimicrobial activity correlated with the density of quaternary ammonium groups present in samples.[16]

Thus, we synthesized an array of immobilized *N*-alkyl-PEI slides containing alkyl groups of various lengths, including two with anionic functional groups and measured their anti-

influenza activity to establish any structure-activity relationships. Virucidal testing was performed against two influenza virus strains pathogenic to humans, influenza A/PR/8/34 (H1N1) and influenza A/Wuhan/359/95 (H3N2), and a laboratory strain, influenza A/WSN/33 (H1N1).

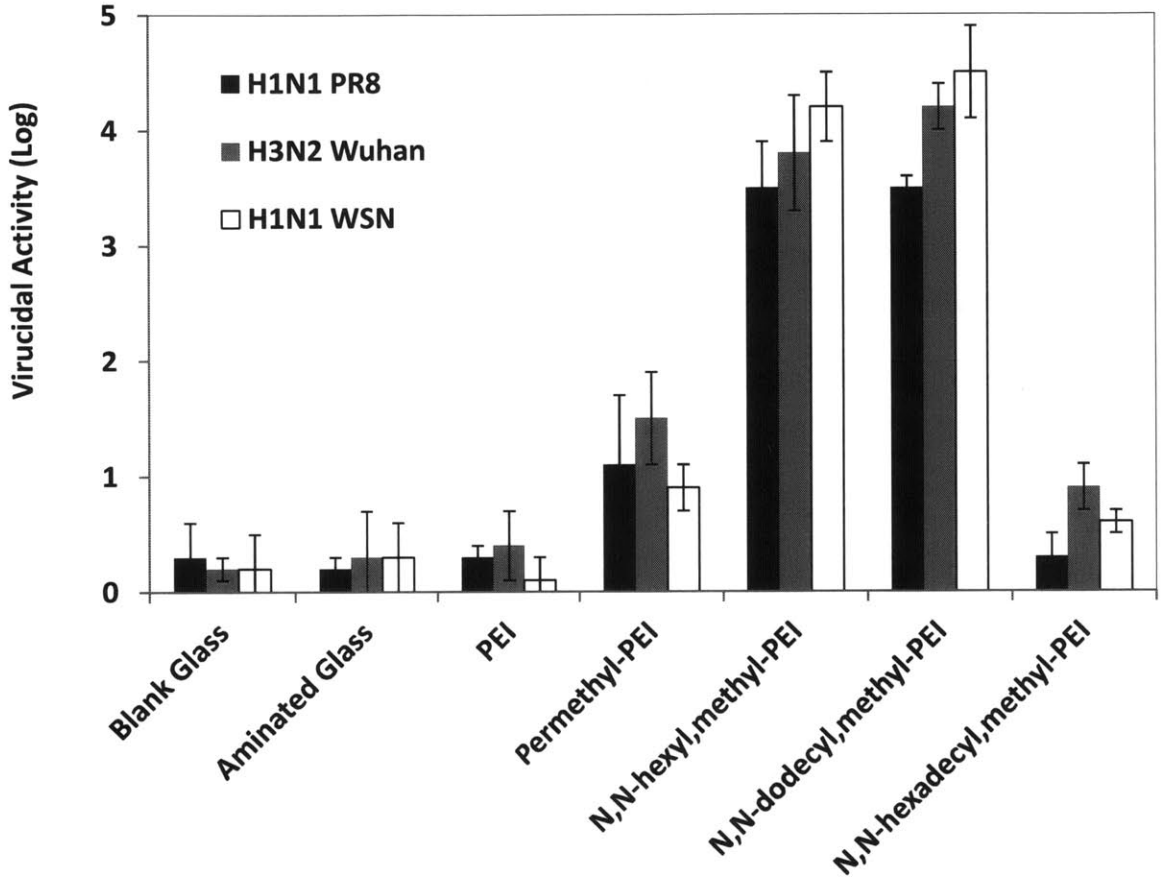

Figure 1. Virucidal activities of *N*-alkyl-PEI surfaces against influenza viruses as a function of alkyl-chain length.

Virucidal assays of the *N*-alkyl-PEI slides against H1N1 PR8, H3N2 Wuhan, and H1N1 WSN revealed that virucidal activity (against all strains) consistently changes depending on the alkyl moiety attached (**Fig. 1**), with highest killing observed (>3.5 log) for *N,N*-hexyl,methyl-PEI and *N,N*-dodecyl,methyl-PEI treated slides.

To understand why the anti-influenza activity varied contingent on alkyl moiety (**Fig. 2**), we then identified various physical-chemical parameters which may correlate with the viral killing ability of the surfaces. Hydrophobicity, average and localized surface charge, quaternary ammonium group density, surface roughness, and polymer chain lengths were measured and linearly correlated with virucidal activity to identify surface properties which most relate to anti-influenza efficacy.

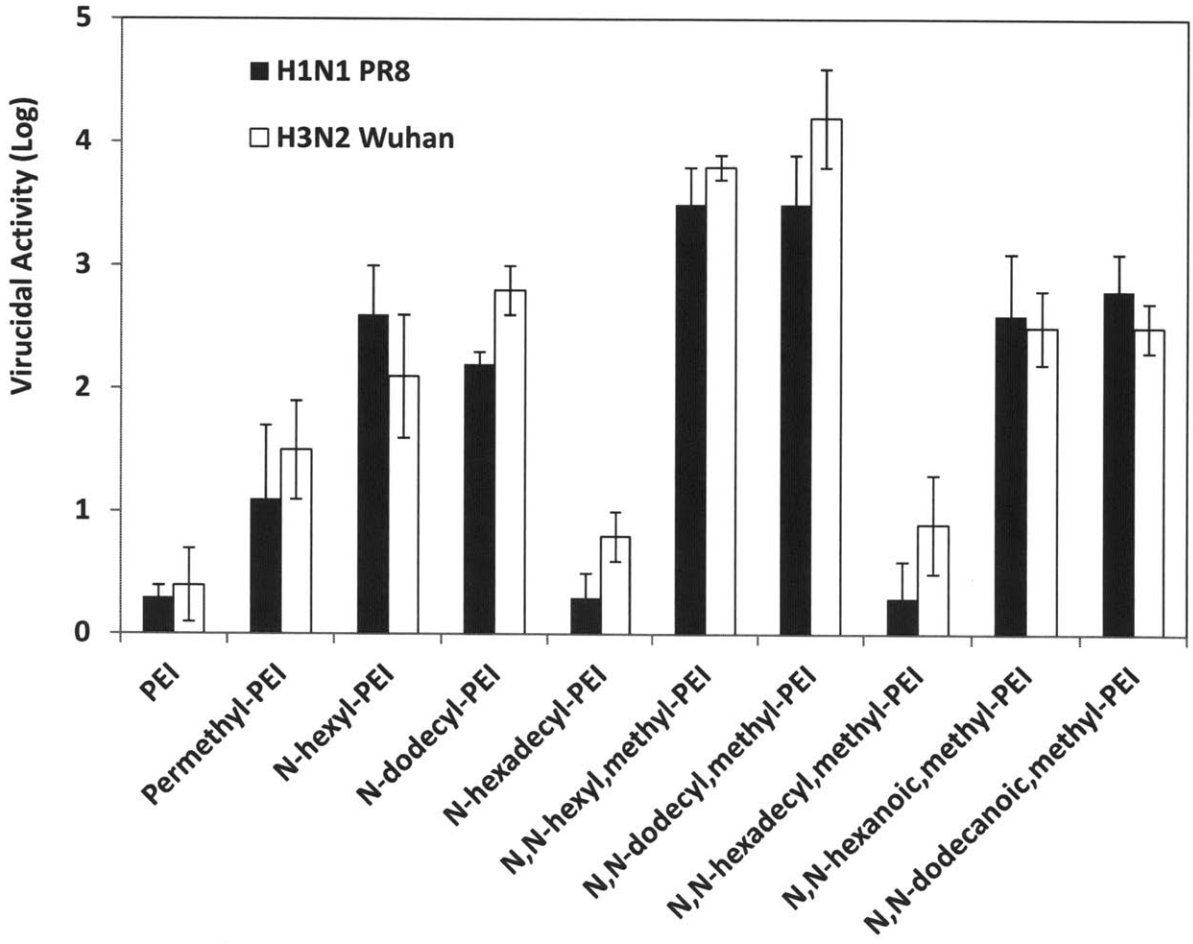

Figure 2. Virucidal activities of *N*-alkyl-PEI surfaces with varying degrees of alkylation.

Hydrophobicity - We used contact angle as a measure of average surface hydrophobicity. Measurements showed increasing contact angles as the length of alkyl chain increased as might be predicted. However, correlating these measurements with virucidal activities yielded a poor correlation coefficient (**Fig. 3**), thus indicating that the virucidal activity does not solely depend on hydrophobicity of the surface.

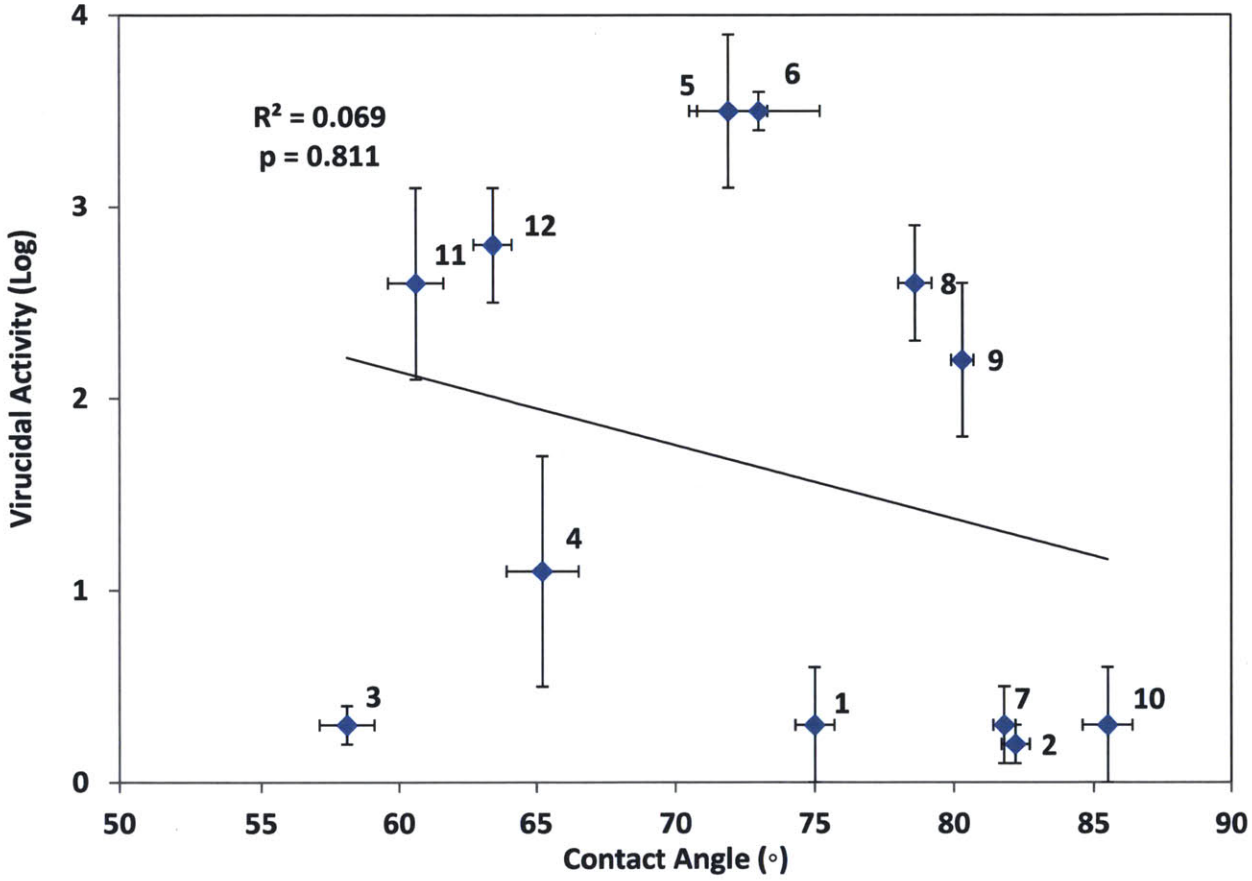

1	Blank Glass Slide	7	*N,N*-hexadecyl,methyl PEI
2	NH_2 Glass Slide	8	*N*-hexyl PEI
3	PEI	9	*N*-dodecyl PEI
4	Permethyl PEI	10	*N*-hexadecyl PEI
5	*N,N*-hexyl,methyl PEI	11	*N,N*-hexanoic,methyl PEI
6	*N,N*-dodecyl,methyl PEI	12	*N,N*-dodecanoic,methyl PEI

Figure 3. H1N1 PR8 Virucidal Activity vs. Contact Angle Correlation

Surface Charge - We used surface zeta potential as a measure of average surface charge. While there was a trend in decreasing surface charge as the length of attached alkyl moiety increased, no significant linear correlation was obtained when plotted against virucidal activity. Therefore the average surface charge of the immobilized polymers does not solely determine virucidal activity. Using contact force AFM to measure localized surface charge, we found that there was no discernible trend with the length of alkyl group attached, and no correlation with virucidal activity (**Fig. 4**). Thus surface charges, both macroscopic and in the micro- to nanometer domain, do not directly influence surface virucidal activity against influenza virus.

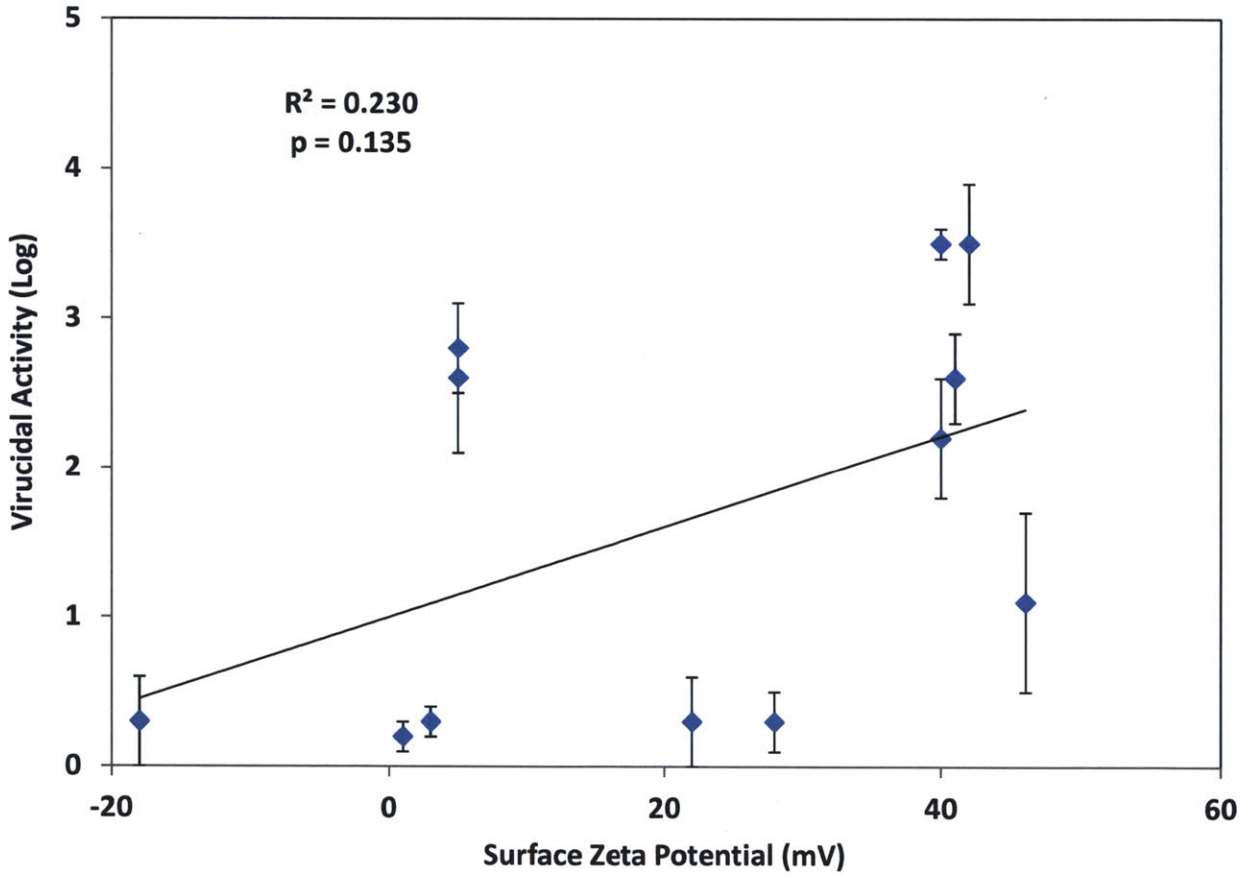

Figure 4. H1N1 PR8 Virucidal Activity vs. Surface Zeta Potential Correlation

Quaternary Ammonium Group Density - Fluorescein titration has been previously used to determine quaternary ammonium density on surfaces. Fluorescein was used to measure the QA groups present on the *N*-alkyl-PEI surfaces. The QA density was determined to be highest for *N,N*-hexyl,methyl-PEI and *N,N*-dodecyl,methyl-PEI, while other PEIs had lower QA densities. The correlation between virucidal activity and the QA density was better than those found with others, yet not entirely significant (**Fig. 5**). Thus, we postulated that the degree of accessibility to QA groups by virus and by fluorescein was different due to physical size. Attaching fluorescein to a larger entity may more closely approximate influenza interaction with QA groups and thus result in an improved correlation.

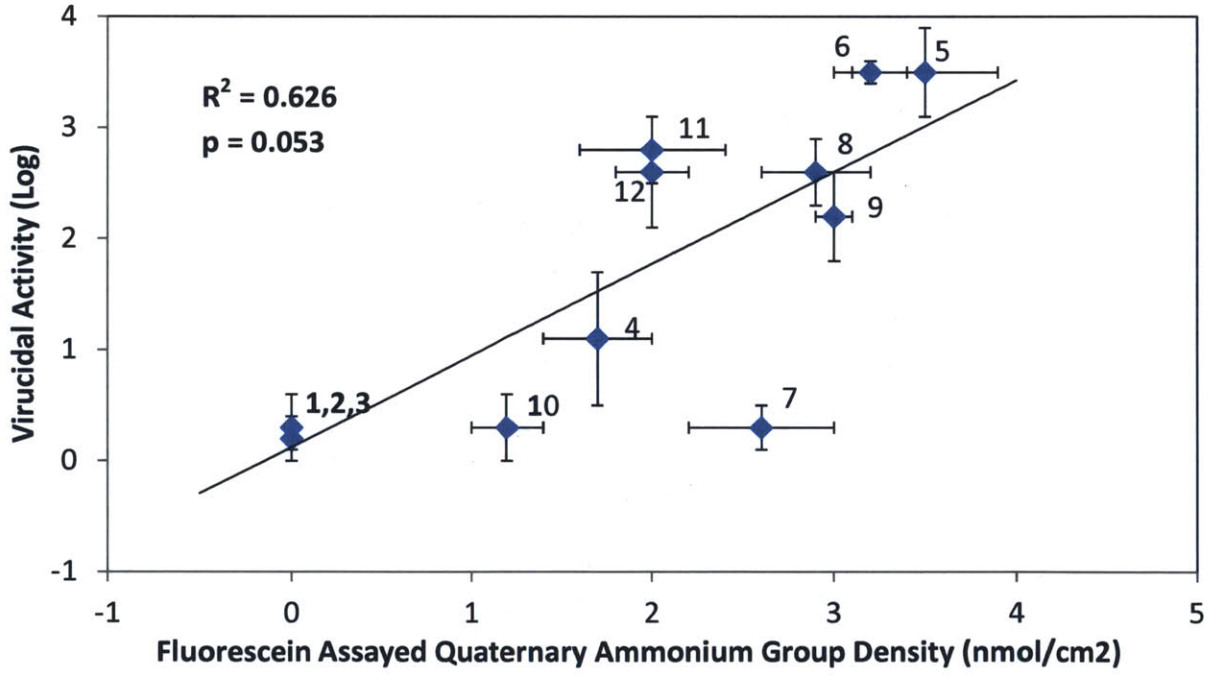

Figure 5. H1N1 PR8 Virucidal Activity vs. Quaternary Ammonium Group Density Correlation

1	Blank Glass Slide	7	*N,N*-hexadecyl,methyl PEI
2	NH_2 Glass Slide	8	*N*-hexyl PEI
3	PEI	9	*N*-dodecyl PEI
4	Permethyl PEI	10	*N*-hexadecyl PEI
5	*N,N*-hexyl,methyl PEI	11	*N,N*-hexanoic,methyl PEI
6	*N,N*-dodecyl,methyl PEI	12	*N,N*-dodecanoic,methyl PEI

Surface Roughness - AFM in tapping mode was used to determine the features of generated *N*-alkyl-PEI surfaces. Three parameters of the scanned surfaces were then used to quantify surface roughness; Ra (average surface roughness), Rrms (root-mean squared surface roughness), and Z-range (largest vertical span over entire surface). No trends were identified between length of alkyl moieties and roughness parameters of each surface. Correlating surface roughness measurements with the activities did not result in good correlation coefficients (**Fig. 6-8**).

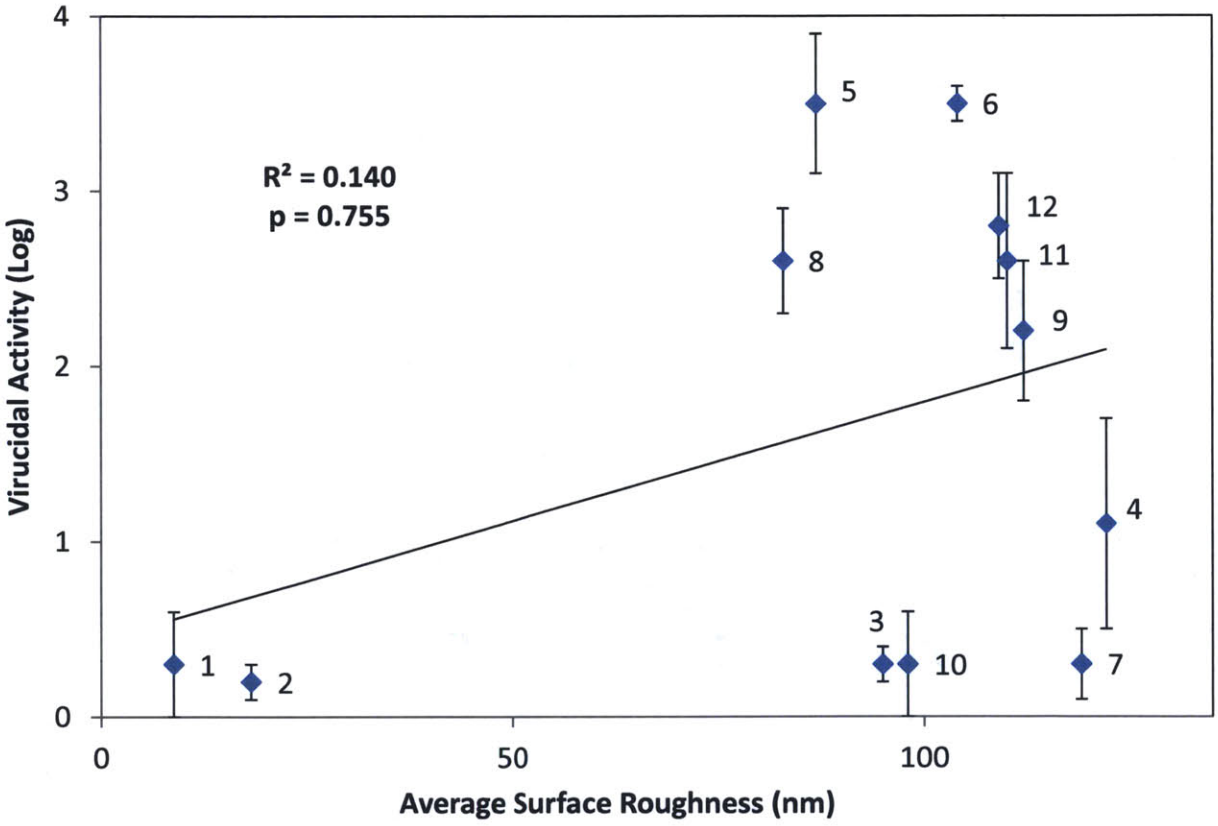

1	Blank Glass Slide	7	*N,N*-hexadecyl,methyl PEI
2	NH_2 Glass Slide	8	*N*-hexyl PEI
3	PEI	9	*N*-dodecyl PEI
4	Permethyl PEI	10	*N*-hexadecyl PEI
5	*N,N*-hexyl,methyl PEI	11	*N,N*-hexanoic,methyl PEI
6	*N,N*-dodecyl,methyl PEI	12	*N,N*-dodecanoic,methyl PEI

Figure 6. H1N1 PR8 Virucidal Activity vs. Average Surface Roughness Correlation

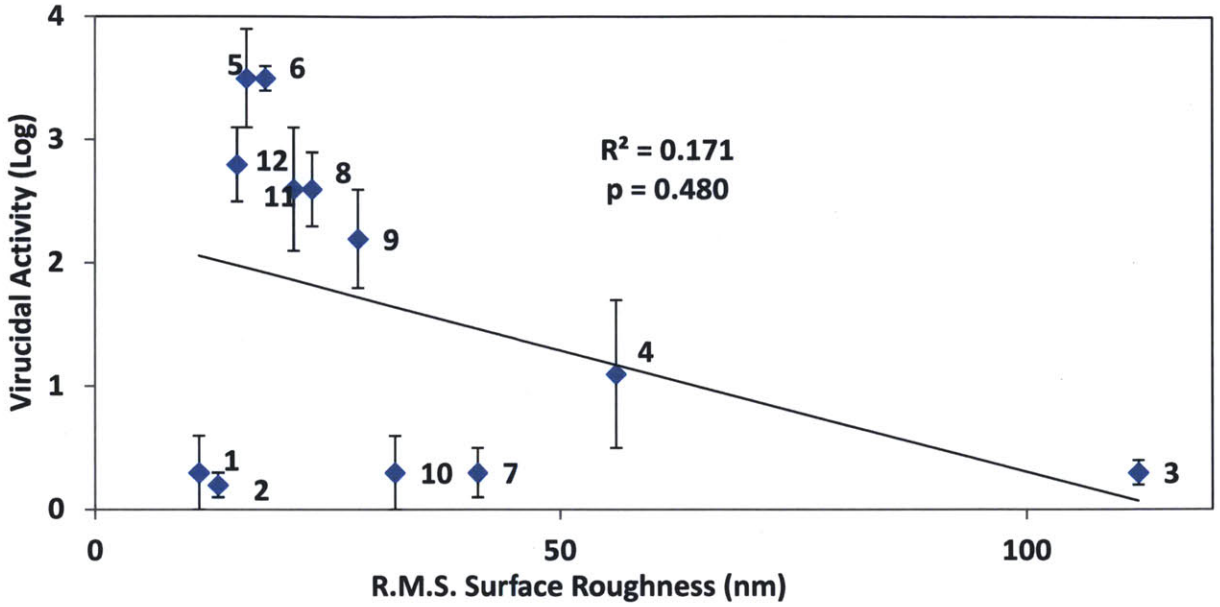

1	Blank Glass Slide	7	*N,N*-hexadecyl,methyl PEI
2	NH_2 Glass Slide	8	*N*-hexyl PEI
3	PEI	9	*N*-dodecyl PEI
4	Permethyl PEI	10	*N*-hexadecyl PEI
5	*N,N*-hexyl,methyl PEI	11	*N,N*-hexanoic,methyl PEI
6	*N,N*-dodecyl,methyl PEI	12	*N,N*-dodecanoic,methyl PEI

Figure 7. H1N1 PR8 Virucidal Activity vs. R.M.S. Surface Roughness Correlation

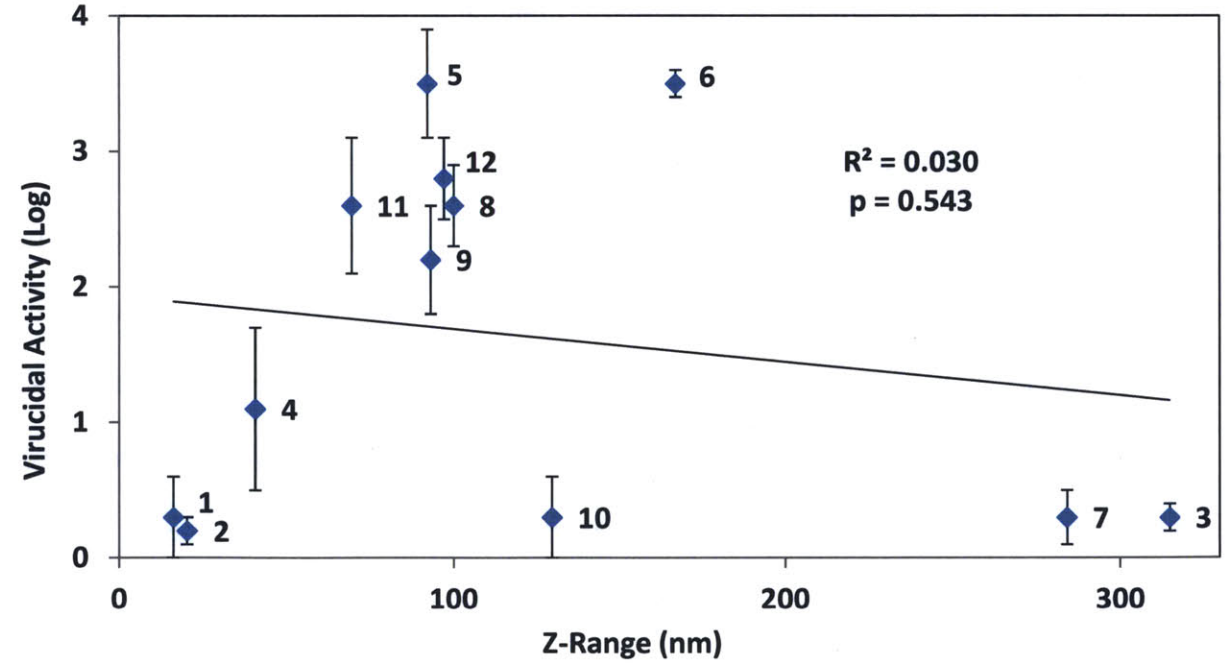

Figure 8. H1N1 PR8 Virucidal Activity vs. Z-range Correlation

Apparent Polymer Length - AFM contact force was also used to determine polymer chain extension distances for each alkyl-PEI surface, as have been used previously.[14] These measurements showed that the alkylated PEIs extended roughly the same distances from the surface. No correlation between the virucidal activities and the polymer chain extension lengths was found.

FITC-Lysozyme Adsorption - In order to test the hypothesis that attaching fluorescein to a larger entity would improve the correlation with virucidal activity, fluorescein isothiocyanate was attached to lysozyme. Lysozyme, at 14 kDa, might more closely mimic an influenza virus than fluorescein. The resulting lysozyme with fluorescein isothiocyanate attached (FITC-Lys) was purified and determined to have a 2:1 ratio of fluorescein to lysozyme with a extinction coefficient of 63200 $M^{-1}cm^{-1}$. Using the same procedures employed with the fluorescein titration, adsorption of FITC-Lys to each *N*-alkyl PEI slide was measured. The resulting correlation between virucidal activities and adsorbed FITC-Lys improved markedly (**Fig. 9**), thus demonstrating that the accessibility of quaternary ammonium groups to influenza virus is a principal determinant of immobilized *N*-alkyl-polyethylenimine virucidal activity. We further controlled for non-specific adsorption of lysozyme by desorbing adsorbed lysozyme from *N*-alkyl-PEI slides with detergent and testing the washings with a Bradford assay, upon which showed no correlation with anti-influenza activity. We also modified lysozyme with a non-QA binding fluorescein analog , rhodamine-B isothiocyanate, and also demonstrated that there was no correlation (**Fig. 10**), further reinforcing the claim that the accessibility of quaternary ammonium groups to influenza virus is the primary determinant of anti-influenza activity. Further experiments may reveal why virucidal activity is dependent on the presence of QA groups, and what mechanism(s) underlie this inactivation of influenza.

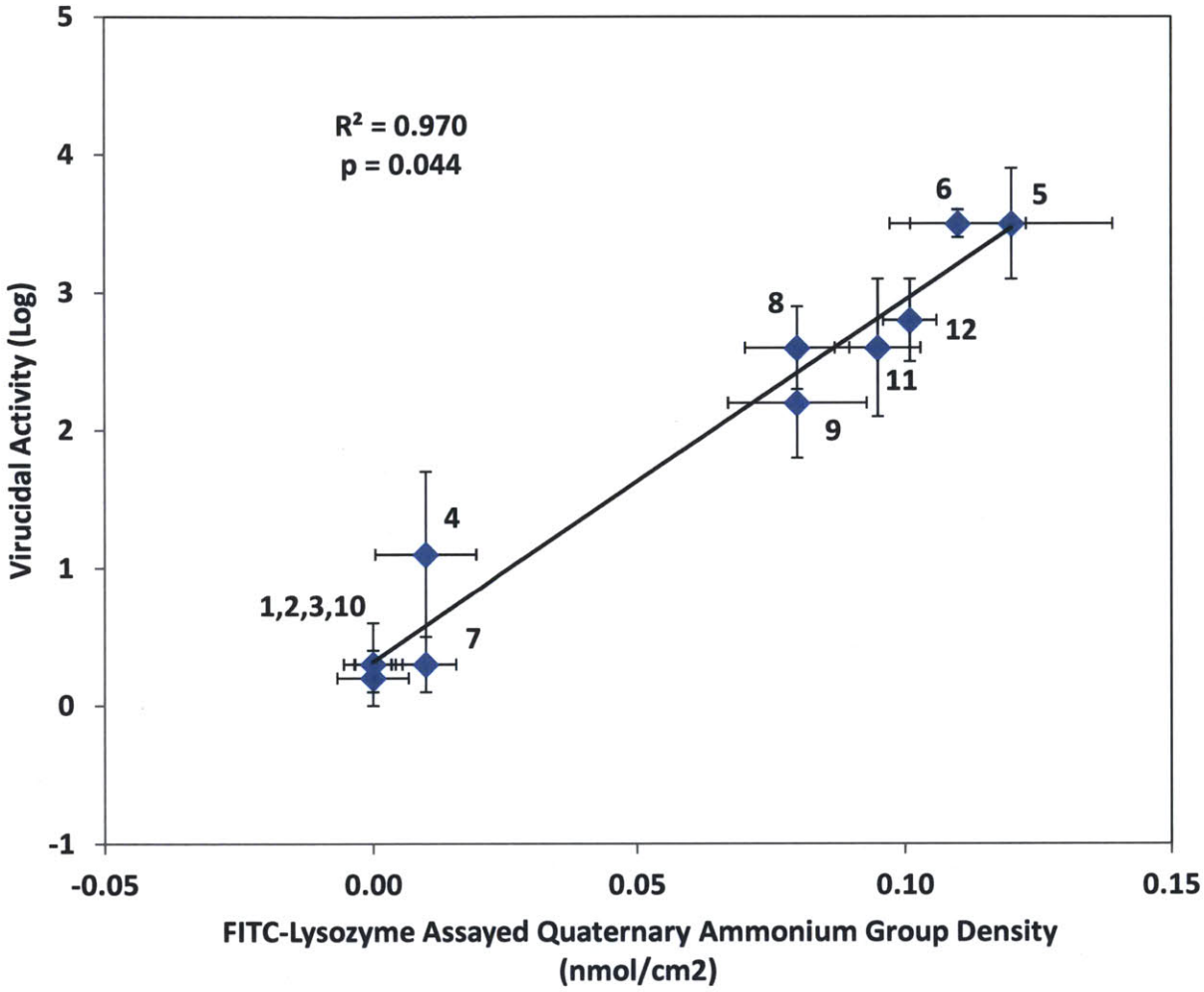

1	Blank Glass Slide	7	*N,N*-hexadecyl,methyl PEI
2	NH_2 Glass Slide	8	*N*-hexyl PEI
3	PEI	9	*N*-dodecyl PEI
4	Permethyl PEI	10	*N*-hexadecyl PEI
5	*N,N*-hexyl,methyl PEI	11	*N,N*-hexanoic,methyl PEI
6	*N,N*-dodecyl,methyl PEI	12	*N,N*-dodecanoic,methyl PEI

Figure 9. H1N1 PR8 Virucidal Activity vs. FITC-Lysozyme Adsorption Correlation

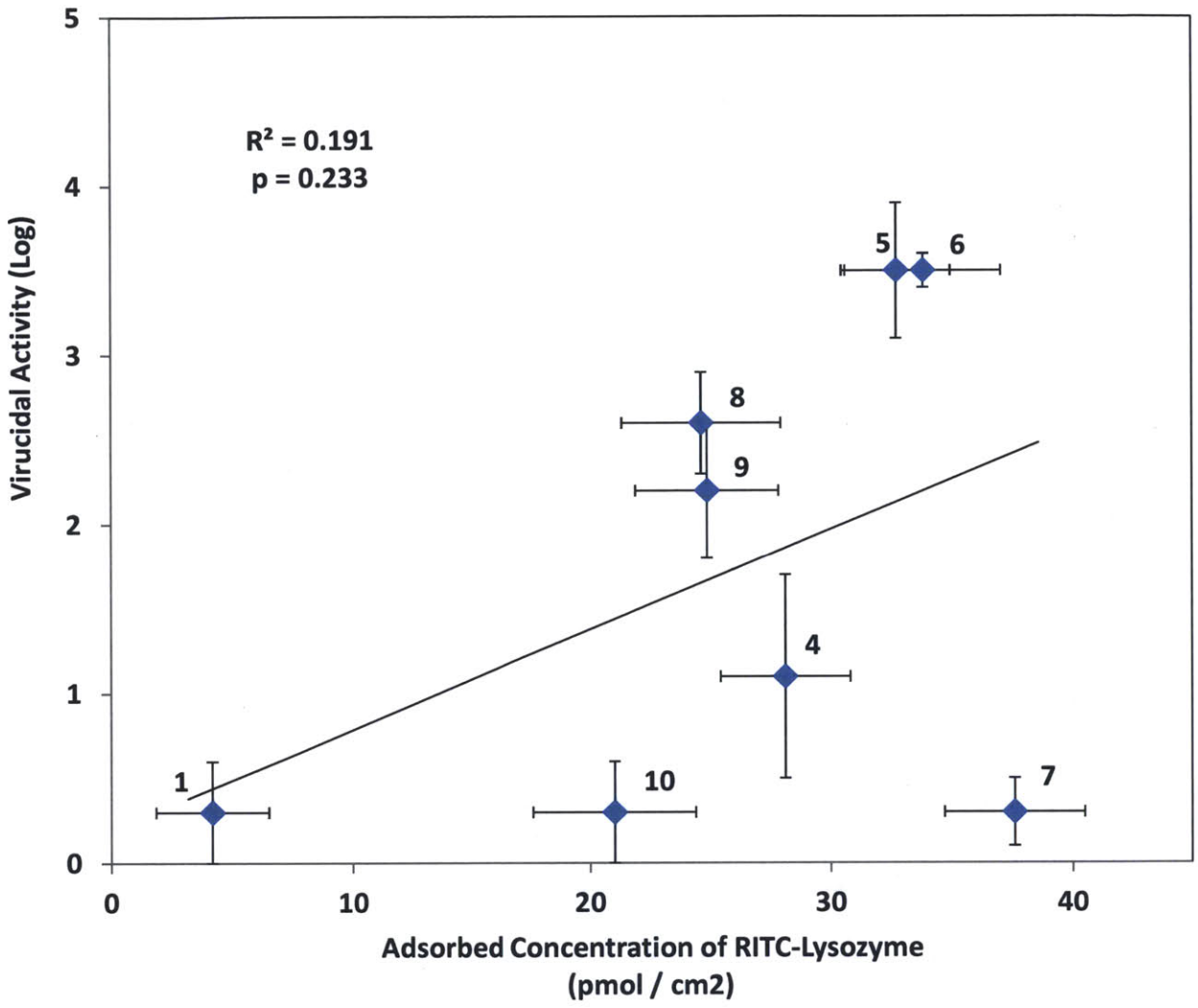

1	Blank Glass Slide	7	*N,N*-hexadecyl,methyl PEI
2	NH_2 Glass Slide	8	*N*-hexyl PEI
3	PEI	9	*N*-dodecyl PEI
4	Permethyl PEI	10	*N*-hexadecyl PEI
5	*N,N*-hexyl,methyl PEI	11	*N,N*-hexanoic,methyl PEI
6	*N,N*-dodecyl,methyl PEI	12	*N,N*-dodecanoic,methyl PEI

Figure 9. H1N1 PR8 Virucidal Activity vs. RITC-Lysozyme Adsorption Correlation

Conclusion

We have revealed that virucidal activities of *N*-alkyl-PEI surfaces are dependent on their specific alkyl modification, and that the activities are highest for specific alkyl chain lengths (6 to 12 carbons). Additionally, we have shown that anti-influenza activity of these surfaces is correlated with accessibility of surface quaternary ammonium groups to influenza virus.

References

1. World Health Organization - Influenza Fact Sheet N°211; 7 August 2014. Available from: **http://www.who.int/mediacentre/factsheets/fs11/en/**
2. Mubareka, S.; Lowen, A.C.; Steel, J.; Coates, A.L.; García-Sastre, A.; Palese, P. *J. Infect. Dis.* **2009**, *199*, 858-865
3. Cowan, M.M.; Abshire, K.Z.; Houk, S.L.; Evans, S.M. *J. Ind. Microbiol. Biotechnol.* **2003**, *30*, 102-106
4. Lin, J.; Tiller, J.C.; Lee, S.B.; Lewis, K.; Klibanov, A.M. *Biotechnol. Lett.* **2002**, 24, 801-805
5. Timofeeva, L.; Kleshcheva, N. *Appl. Microbiol. Biotechnol.* **2011**, *89*, 475-492
6. Haldar, J.; An, D.; de Cienfuegos, L. A.; Chen, J.; Klibanov, A.M. *Proc. Natl. Acad. Sci. U.S.A.* **2006**, *103,* 17667-17671
7. Haldar, J.; Chen, J.; Tumpey, T.M.; Gubareva, L.V.; Klibanov, A.M. *Biotechnol. Lett.* **2008**, *30*, 475-479
8. Liu, H.; Kim, Y.; Mello, K.; Lovaasen, J.; Shah, A.; Rice, N.; Yim, J.; Pappas, D.; Klibanov, A.M. *Appl. Biochem. Biotechnol.* **2014**, *172*, 1254-1264
9. Hsu, B.B.; Wong, S.Y.; Hammond, P.T.; Chen, J.; Klibanov, A.M. *Proc. Natl. Acad. Sci. U.S.A.* **2011**, *108*, 61-66
10. Thomas, M.; Lu, J.J.; Ge, Q.; Zhang, C.; Chen, J.; Klibanov, A.M. *Proc. Natl. Acad. Sci. U.S.A.* **2005**, *102*, 5679-5684
11. Hiramatsu, M.; Okabe, N.; Tomita, K. *J. Biochem.* **1973**, *73,* 971-978
12. McDonagh, P. F.; Williams, S. K. *Microvasc. Res.* **1984**, *27,* 14-27
13. Lin, J.; Qiu, S.; Lewis, K.; Klibanov, A.M. *Biotechnol. Bioeng.* **2003**, *83*, 168-172
14. Iarikov, D.D.; Kargar, M.; Sahari, A.; Russel, L.; Gause, K.T.; Behkam, B.; Ducker, W.A. *Biomacromolecules*, **2014**, *15*, 169-176
15. Haldar, J.; Weight, A.K.; Klibanov, A.M. *Nat. Protoc.* **2007**, *2*, 2412-2417
16. Huang, J.; Koepsel, R.; Murata, H.; Wu, W.; Lee, S.B.; Kowalewski, T.; Russell, A.J.; Matyjaszewski, K. *Langmuir* **2008**, *24*, 6785-6795
17. Murata, H.; Koepsel, R.R.; Matyjaszewski, K.; Russell, A.J. *Biomaterials* **2007**, *28*, 4870-4879
18. Thomas, M.; Lu, J.J.; Ge, Q.; Zhang, C.; Chen, J.; Klibanov, A.M. *Proc. Natl. Acad. Sci. U.S.A.* **2005**, *102*, 5679-5684

19. Tiller, J.C.; Liao, C.J.; Lewis, K.; Klibanov, A.M. *Proc. Natl. Acad. Sci. U.S.A.* **2001**, *98*, 5981-5985
20. Wong, S.Y.; Han, L.; Timachova, K.; Veselinovic, J.; Hyder, M.N.; Ortiz, C.; Klibanov, A.M.; Hammond, P.T. *Biomacromolecules* **2012**, *13*, 719-726

Aerosol-assisted plasma deposition of hydrophobic polycations makes surfaces highly antimicrobial

Introduction

Creating non-leaching surfaces which kill pathogenic bacteria and disinfect viruses on contact is important due to the ever-growing increase in multi-drug resistant microbes.[1,2] Previously, we demonstrated that certain hydrophobic polycations based on alkylated polyethylenimines (PEIs) or poly(vinyl pyridines) covalently attached to various solid surfaces efficiently (over 3-log titer reductions) inactivate bacteria and viruses with no resistance developing.[3] However, preparing these covalently-modified antimicrobial surfaces is onerous because it requires harsh reaction conditions, involves multi-step syntheses, and is surface specific.[3]

In order to explore elimination of these practical drawbacks, in this study we have attached *N,N*-hexyl,methyl-PEI (HMPEI) to a solid surface by alternative, new means using an Invexus™ technology — an atmospheric-pressure plasma liquid deposition process.[4,5,6] This method provides a potential route to covalent immobilization of HMPEI via a facile and readily scalable one-step process, which should be surface-independent. The resultant coatings yield surfaces that are nanometer-thin, conformal, durable, wash resistant, thermally stable, and highly antimicrobial.

Materials and Methods

Chemicals and Biologicals

Microscope glass slides (75 × 25 × 1 mm) were purchased from Corning Inc. (Corning, NY). Branched PEI (50% (w/w) aqueous solution, average molecular weight of 50,000 g/mol) and other chemicals and solvents were purchased from Sigma-Aldrich Chemical Co. (St. Louis, MO) and used without further purification. HMPEI was synthesized as previously described.[7] *Escherichia coli* (ATCC 8739) and Madin-Darby canine kidney (MDCK) cells were obtained from the ATCC (Manassas, VA). The bacterial cells were grown in Luria-Bertani (LB) broth, Lennox (Becton, Dickinson and Co., Franklin Lakes, NJ). Influenza A/PR/8/34 (H1N1) virus was obtained from Charles River Laboratories (Wilmington, MA).

Atmospheric Pressure Plasma Liquid Deposition (APPLD)

HMPEI was deposited using the Invexus™ technology, an atmospheric-pressure plasma liquid deposition process utilizing a non-thermal plasma to polymerize and covalently bond precursor monomers onto surfaces. Specifically, a batch-to-batch platform, SE2100™ Jet PlasmaStream Workstation,[4,5] was used. Briefly, the device consists of a plasma deposition head (Figure 1) where the plasma generation and precursor atomization take place, and a computer controlled x-y-z table is used to move the deposition system relative to the surface to be coated. The plasma deposition head utilizes a 19-mm internal-diameter tubular nozzle assembly containing high-voltage RF electrodes that ionize the flowing inert gas and direct the resultant plasma discharge onto the targeted surface. The liquid precursors are introduced via a pneumatic nebulizer as an atomized liquid directly into the plasma discharge within the tubular nozzle. The combination of free-radical and ionized-plasma species activates the liquid precursors

sufficiently to initiate surface modification but without significant fragmentation and re-arrangement of the molecules, resulting in nanometer-thick coatings on the targeted surface. The plasma also ensures that the coating is chemically bonded to the surface due to its simultaneous activation during the deposition process.

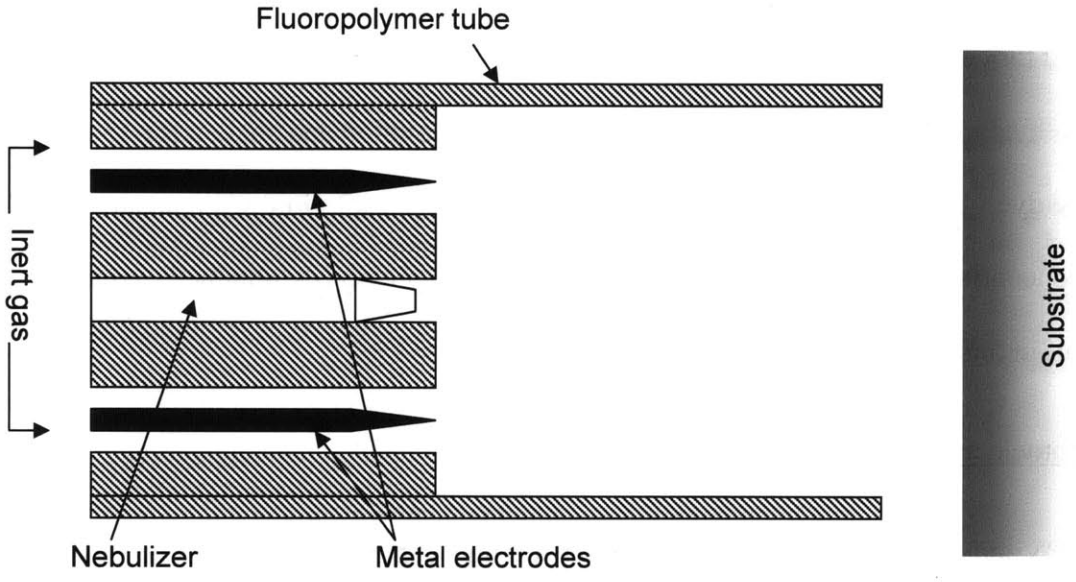

Figure 1. Schematic diagram of the plasma head (modified from O' Neill, 2009).

For the deposition process, 5% (w/w) HMPEI in ethanol was used as a precursor solution which was delivered to the atomizer at a rate of 15 μL/min with inlet pressure of 50 psi at room temperature. A frequency of 20 kHz with peak voltages of 19.5 to 21.0 kV was used for power supply. Helium was used as the inert gas at a rate of 15 L/min. The target surface explored herein was that of soda lime glass slides which were used as obtained commercially or cut into 10 × 25 mm rectangular pieces. The gap between the nozzle and the surface was approximately 0.5 mm. The plasma deposition head moved at a scan rate of 30 mm/sec, and the gap between raster scans

was 1 mm. The glass surfaces were scanned either 10 or 20 times; for a 75 × 25 mm glass slide, one pass takes approximately 66 sec.

Analysis of Quaternary Ammonium Groups

A HMPEI-coated glass slide (55 x 25 mm) was shaken in a 1% solution of fluorescein Na salt in phosphate-buffered distilled water (0.1 M NaH_2PO_4, pH 8.0) for 15 min. The slide was then rinsed thrice with the dye-free buffered solution before being placed in 45 mL of 0.1% cetyltrimethylammonium chloride in this aqueous buffer solution and shaken for 15 min to desorb the dye.[8] The light absorbance of the resultant aqueous solution was measured at 501 nm, and the concentration of the dye was determined using the previously obtained extinction coefficient in this solution of 77 $mM^{-1}cm^{-1}$.[9]

X-ray Photoelectron Spectroscopy (XPS)

XPS analysis was used to determine the coatings composition and, more specifically, the nitrogen content of the HMPEI coatings. A Kratos Axis Ultra XPS system equipped with a hemispherical analyzer and a 100 W monochromatic Al Kα (1486.7 eV) beam was used. This analysis was performed on 1 × 0.5 mm sampling area at a take-off angle of 90°. The base pressure in the XPS chamber was held between 10^{-9} and 10^{-10} Torr. Survey scans and elemental high-resolution scans for C 1s and N 1s were taken in the constant analyzer energy mode of 80 and 20 eV pass energy, respectively. Corrected binding energy for the C 1s and N 1s spectra were set to 285.0 and 399.6 eV, respectively, corresponding to the aliphatic carbon-carbon and the nitrogen-hydrogen, respectively. Deconvolution of high-resolution C 1s and N 1s spectra was carried out through a CasaXPS software using a Gaussian-Lorentzian fit and a full-width half-maximum (FWHM) of 1.6 or less. A total of four spots were scanned for each sample.

Contact Angle and Profilometry

The wettability of the HMPEI-coated glass surfaces was assessed through water contact angles based on the sessile-drop method. Contact angles were measured using a FTA-1000B contact angle and surface tension instrument (First Ten Angstroms, Inc., Portsmouth, VA). The volume of the water droplet was 5 μL. The HMPEI coating thickness was measured using a XP-1High-Resolution Surface Profiler profilometer (AmBios Technology, Inc., Santa Cruz, CA). The coated surfaces were scanned for 2.00 mm at a scan speed of 0.01 mm/sec and stylus force of 0.05 mg.

Durability Test

Plasma-coated glass slides were rinsed thrice with distilled water and then shaken overnight in a 1% Liquinox anionic detergent solution at 55°C. This treatment was followed by rinsing the slides thrice with distilled water again and then titrating them with fluorescein as described above. The quaternary ammonium group densities were subsequently compared with those of the pre-washed samples to determine whether the titer had decreased due to washing.

Bactericidal and Virucidal Activities

An overnight culture of *E. coli* was spun down in a centrifuge tube, and the supernatant was discarded. Phosphate-buffered saline solution (PBS) was then added to the tube, and the cell pellet was re-suspended. Centrifugation and re-suspension steps were repeated, and the final *E. coli* solution was diluted to approximately 6×10^6 CFU/mL with PBS. This diluted bacterial solution (10 μL) was inoculated onto a coated glass slide (10 × 25 mm), and an uncoated glass slide of the same size was placed on top to spread the inoculum. After a 2-h incubation, the slides

were transferred into centrifuge tubes with 10 mL of an extraction solution (0.5% (w/v) lecithin and 4% (w/v) Tween 20 in PBS). The tubes were vortexed to separate the slides. The extraction solution was subsequently plated to determine CFU counts.

Virucidal activity was determined as previously described.[10] Briefly, a 10-μL droplet of an influenza virus solution (approximately 10^8 PFU/mL) was placed in the center of a coated glass slide (25 × 25 mm). A non-coated glass slide was then used to cover and spread the droplet. After a 10-min incubation, the virus-exposed sides of both slides were washed with 0.99 mL of PBS. Two-fold serial dilutions of the washings were then made with PBS, and 200 μL of each dilution was subsequently added to confluent MDCK cells in 6-well tissue culture plates to determine plaque counts.

Thermal Stability of HMPEI Coatings

The HMPEI-coated glass slides were exposed to 90 °C or 150 °C for 2 h in an oven and then tested for antimicrobial activity to determine thermal stability of the coatings. Differential scanning calorimetry (DSC) (Q20, TA Instruments, New Castle, DE) of the raw precursor of HMPEI (not of the resultant coatings) was performed by equilibrating it at -40 °C, heating it up to 150 °C at 10 °C/min, holding it at 150 °C for 0.25 min (the first scan), cooling it to -40 °C at 10 °C/min, holding it at -40 °C for 0.25 min, and heating it up to 150 °C at 10 °C/min (the second scan).

Results and Discussion

The goal of this study was to explore a new, single-step procedure for attaching hydrophobic polycations, as exemplified by HMPEI, to solid surfaces using atmospheric-pressure plasma liquid deposition. A key benefit of the facile plasma deposition process used herein is that a degradation of the precursor molecules (HMPEI in this case) in the plasma is minimized by introducing it as a liquid aerosol into a non-thermal plasma.[4] Consequently, the resultant coating retains the chemical structure of the precursor molecules, thus achieving characteristics similar to those reported for pulsed-vacuum plasmas[12,13] or in wide-area aerosol-assisted atmospheric-pressure plasma coatings.[6] Also, exposure to the He discharge leads to further cleaning of the target surface, followed by plasma-induced functionalization that promotes better adhesion of the coating. Furthermore, the deposition process takes place at room temperature making it suitable for a variety of surfaces, including those of soft materials.

The extent of plasma coating of glass slides with HMPEI was initially characterized by quantifying the surface density of the grafted quaternary ammonium groups using a fluorescein assay. As seen in Table 1 (first data column), 4.7 nmol/cm^2 of quaternary ammonium group were introduced after 10 plasma-coating passes each lasting about a minute or less. This value has not changed appreciably after 10 additional plasma coating cycles (Table 1) indicating that saturation of the surface was already achieved. Importantly, these quaternary ammonium group densities were comparable to those determined by us previously for glass slides covalently derivatized using the conventional 5-step surface-specific chemical synthesis.[9]

Table 1. Quaternary ammonium group densities of glass slides plasma-coated with HMPEI before and after detergent washing as a function of the number of coating passes.

No. of passes	Quaternary ammonium group density (nmol/cm^2)	
	Before wash	After wash
Uncoated	0	0
10	4.7 ± 0.3	4.6 ± 0.4
20	4.5 ± 0.4	4.5 ± 0.4

To assess the robustness of the surface-immobilized HMPEI prepared herein, we subjected the plasma-coated glass slides to exhaustive washing with water and a Liquinox detergent at an elevated temperature (55°C). As seen in Table 1 (last column), there was no detectable difference in the quaternary ammonium group densities before and after the washing. These results indicate that plasma deposition of HMPEI results in a covalent attachment, as opposed to a physical adsorption, of the hydrophobic polycations to the glass surface; this conclusion was further confirmed using the detailed surface analysis techniques described below.

Next, surface compositions of the HMPEI coating were investigated by means of XPS analysis. An example of a survey scan for each sample is depicted in Figure 2, and the surface compositions are shown in Table 2. Trace elements not associated with the HMPEI deposition process were identified from XPS and attributed to residue due to handling; therefore, they were disregarded in the elemental considerations of the coatings. As expected, the nitrogen content rose with the number of passes of the plasma-coating process. Likewise, the Br content (from the HMPEI's counter-ion) approximately doubled as the number of coating passes was raised from

10 to 20. Since Br is an artifact from HMPEI synthesis, it is expected to increase similarly to the N content. The Si peaks were from the underlying glass surface. For thin coatings (fewer passes by the plasma-coating process), more intense Si signals from the underlying glass surface were detected in agreement with previous studies of plasma deposition.[4]

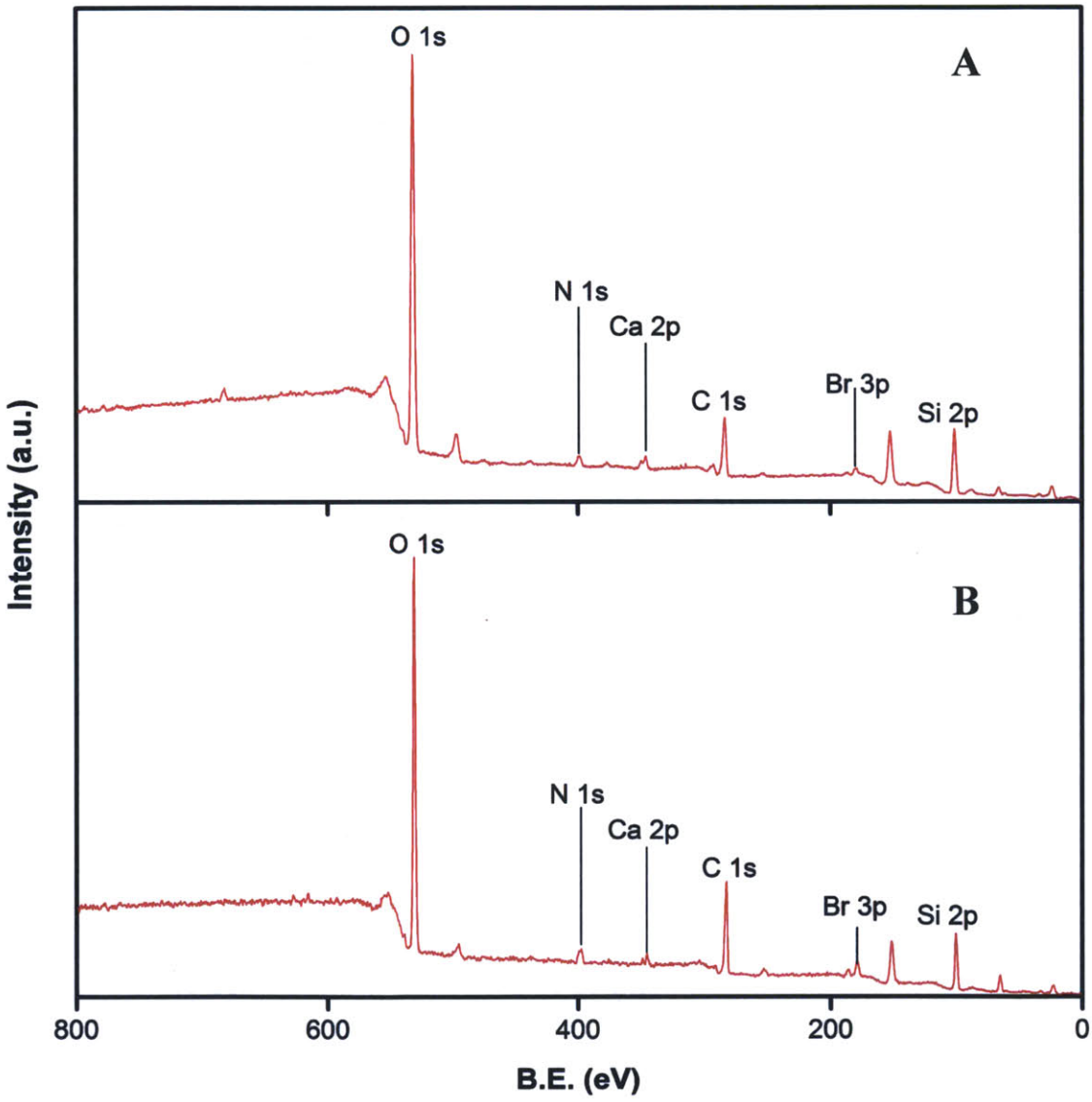

Figure 2. XPS survey spectra of HMPEI coatings deposited on glass slides after 10 passes (**A**) and 20 passes (**B**).

Table 2. The surface composition of HMPEI coating on glass slides after 10 and 20 plasma coating passes.

Number of passes	Spot no.	Atomic content (%)					
		C 1s	O 1s	N 1s	Ca 2p	Br 3p	Si 2p
10	1	23.37	47.98	2.72	0.99	0.89	24.05
	2	23.39	51.27	2.40	1.11	0.66	21.17
	3	24.03	46.34	2.53	0.92	0.75	25.44
	4	21.95	50.49	3.30	0.76	1.09	22.39
	Avg.	23.19	49.02	2.74	0.95	0.85	23.26
20	1	37.05	37.01	4.77	0.53	2.08	18.56
	2	34.70	42.15	4.57	0.37	2.13	16.09
	3	38.43	36.40	4.48	-	2.65	18.04
	4	39.35	35.17	4.88	0.38	1.85	18.37
	Avg.	37.38	37.68	4.68	0.43	2.18	17.77

Table 3. Fitted peak binding energies (B.E.) and chemical group identification.[14,15,16]

Peak no.	B.E. (eV)	Assigned chemical group
C1	284.3	C-Si
C2	285.0	C-C
C3	285.6	C-C-C / C-N
C4	286.5	C-O, C-C-C
C5	287.2	N-C=O
C6	288.6	C=O
N1	399.6	C-N, cyano
N2	401.4	quaternary nitrogen
N3	402.5	$-N^{+}-$, protonated amine

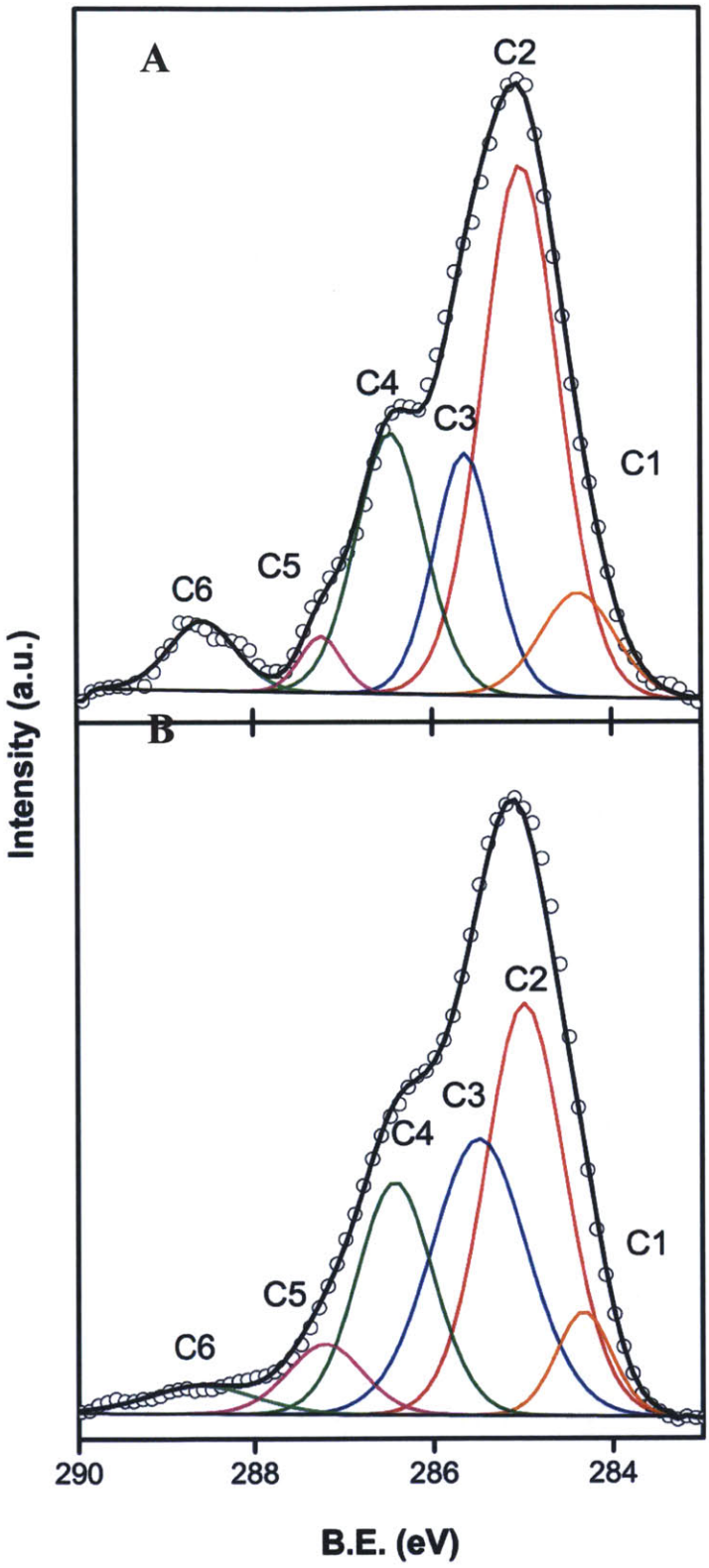

Figure 3. Deconvoluted C1s peak of the HMPEI coatings after 10 passes (**A**) and 20 passes (**B**).

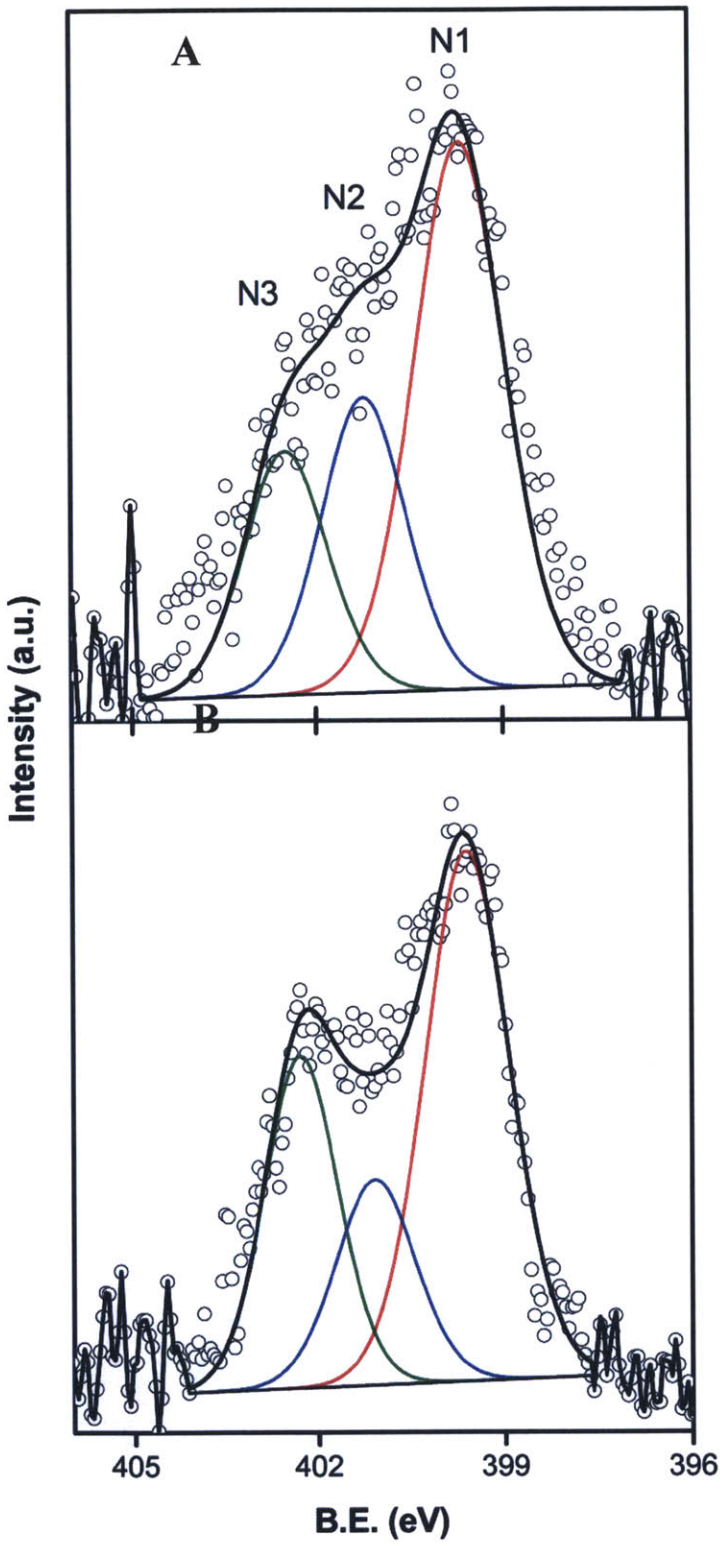

Figure 4. Deconvoluted high-resolution N1s peak of the HMPEI coatings after 10 passes (**A**) and 20 passes (**B**).

To determine the carbon-based functional groups, deconvolution of the C1s peaks was employed, which is depicted in Figure 3. T-fitted peak binding energy (B.E.) and chemical group identifications are listed in Table 3. Of particular note is the presence of the peak at 284.3 eV attributed to a C-Si bond in both samples. This peak further confirms that the coatings are chemically bonded to the glass surface via a direct carbon-to-silicon bond, whose presence explains the high level of wash resistance exhibited by the coatings. In addition, the curve fitting revealed a series of peaks attributed to the hydrocarbon and nitrogen species of the starting hydrophobic polycation, indicating that the functional chemistry of the precursor was retained in the coating. Additional weaker peaks at 287.2 and 288.6 eV (Fig. 3) are attributed to the presence of O in the coating. This may be due to minor oxidation of the precursor HMPEI,[9] or reflect the formation of chemical bonds between the coating and the SiO_x layer, or be a combination of both. The N1s signal peak shape for HMPEI coating deposited over 10 passes is distinct from that deposited over 20 passes. Deconvolution revealed three peaks at 399.6, 401.4, and 402.5 eV, as depicted in Figure 4, corresponding to C-N, quaternary N, and protonated amine groups, respectively. This analysis shows that cationic nitrogen moieties are indeed present in the HMPEI coatings.

As seen from the data in Table 4, the HMPEI coatings were moderately hydrophobic and their thickness was approximately 30 nm. Note that both contact angle and coating thickness were comparable regardless of the number of plasma coating passes.

Table 4. Physical properties of HMPEI coatings.

Number of passes	Contact angle with water[a] (°)	Coating thickness[b] (nm)
10	55.9 ± 1.8	32 ± 19
20	50.3 ± 0.8	34 ± 13

[a] Contact angle was measured once from each sample and averaged from three samples.

[b] Coating thickness was measured in three different locations for each sample and averaged from three samples (a total of 9 measurements).

Having achieved a permanent attachment of HMPEI to the glass surface by plasma deposition and characterized the resultant coatings, we then examined their antimicrobial properties. Bactericidal activity was tested against waterborne *E. coli*. As seen in Table 5 (first data column), the plasma-coated slides afforded an over 2.5-log reduction in the bacterial titer when compared to the uncoated (control) slides under the same conditions. Thus, greater than 99% reduction in bacterial numbers was achieved by both the 10- and 20- pass coating samples (Table 5). This antibacterial potency is comparable to that of the HMPEI immobilized via a conventional 5-step procedure.[9]

Table 5. Antimicrobial efficiencies of glass slides plasma-coated with HMPEI against *E. coli* and influenza viruses as a function of the number of coating passes.

Number of passes	Titer reduction (logs)	
	E. coli	Influenza virus
0 (control)	0	0
10	> 2.8[a]	4.5 ± 0.3
20	> 2.6[a]	4.3 ± 0.4

[a] No bacterial colonies were observed on agar plates, and the numbers given indicate detection limits of the test based on dilutions and plated volumes.

We also assessed the antiviral properties of the HMPEI-coated glass slides against human influenza H1N1 virus. As seen in the last column of Table 5, the plasma-coated slides resulted in a greater than 4-log reduction in the viral titer when compared to the control. These data demonstrate that both antibacterial and antiviral properties of plasma-coated HMPEI slides are at least on par with those previously prepared using multi-step and surface-dependant covalent attachment of this hydrophobic polycation to the same surface.

A 2-h incubation of the immobilized HMPEI, deposited by either 10 or 20 coating passes, at 150 °C resulted in no reduction and, in fact, a slight increase of its antibacterial activity. This observation further attests to good heat resistance of the plasma-deposited hydrophobic polycation.

Table 6. Antimicrobial efficiencies of glass slides plasma-coated with HMPEI after heat treatment against *E. coli* as a function of the number of coating passes.

Number of passes	Titer reduction (logs)	
	After 2 h at 90 °C	After 2 h at 150 °C
0 (control)	0	0
10	1.2 ± 0.4	> 3.2[a]
20	1.7 ± 0.4	3.3 ± 0.4

[a] No colonies were observed on agar plates, and the numbers given indicate the detection limit of the test.

Finally, differential scanning calorimetry was used to probe the thermal properties of the HMPEI prior to its plasma immobilization onto a glass slide. As seen in Figure 5, the hydrophobic polycation features a glass transition temperature (T_g) at approximately 70 °C in the first DSC scan. There was also a broad exotherm between 110 °C and 150 °C, which might indicate some polymer cross-linking in this temperature range. Indeed, a second scan of the same sample showed that the T_g value rose to about 100 °C, indicating a change in properties. It is noteworthy, however, that this putative cross-linking or another molecular re-arrangement had likely occurred upon exposure of the plasma-coated slide to 150 °C for 2 h and, as noted above, no adverse effect on the antibacterial efficacy was observed.

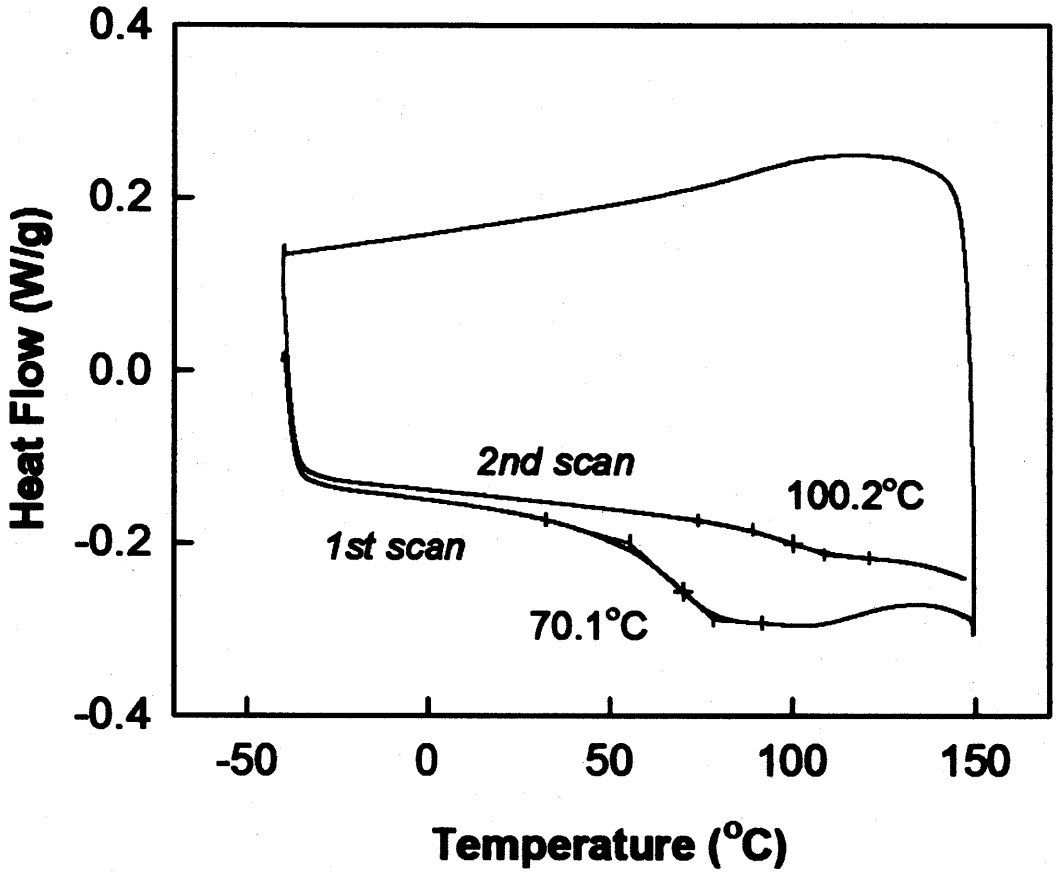

Figure 5. Differential scanning calorimetry of HMPEI.

In closing, in the present work we have examined and validated a facile and scalable atmospheric-pressure plasma liquid deposition method for readily attaching hydrophobic polycationic coatings to a solid surface in a single step to endow it with strong and permanent antimicrobial properties.

Acknowledgment

This research was financially supported by the U.S. Army Research Office under contract W911NF-07-D-0004.

References

1. Horimoto, T., & Kawaoka, Y. (2005). Influenza: lessons from past pandemics, warnings from current incidents. *Nature Revs. Microbiol., 3*, 591-600.

2. Lewis, K. (2007). Persister cells, dormancy, and infectious disease. *Nature Revs. Microbiol., 5*, 48-56.

3. Klibanov, A.M. (2007). Permanently microbicidal materials coatings. *J. Mater. Chem., 17,* 2479-2482.

4. Albaugh, H., O'Sullivan, C., & O'Neill, L. (2008). Controlling deposition rates in an atmospheric pressure plasma system. *Surf. Coat. Technol., 203*, 844-847.

5. O'Neill, L., & O'Sullivan, C. (2009). Polymeric coatings deposited from an aerosol-assisted non-thermal plasma jet. *Chem. Vapor Deposition, 15*, 21-26.

6. Twomey, B., Dowling, D.P., Byrne, G., Graham, W.G., Schaper, L.F., Della Croce, D., Hynes, A., & O'Neill, L. (2009). Comparing deposition properties in an atmospheric pressure plasma system operating in uniform and non-uniform modes. *IEEE Trans. Plasma Sci., 37*, 961-969.

7. Park, D., Wang, J., & Klibanov, A.M. (2006). One-step, painting-like coating procedures to make surfaces highly and permanently bactericidal. *Biotechnol. Progr., 22,* 584-589.

8. Ledbetter, J.W., Jr., & Bowen, J.R. (1969). Spectrophotometric determination of the critical micelle concentration of some alkyldimethylbenzylammonium chlorides using fluorescein. *Analyt. Chem., 41,* 1345-1347.

9. Lin, J., Qiu, S., Lewis, K., & Klibanov, A.M. (2003). Mechanism of bactericidal and fungicidal activities of textiles covalently modified with alkylated polyethylenimine. *Biotechnol. Bioeng., 83,* 168-172.

10. Haldar, J., Weight, A.K., & Klibanov, A.M. (2007). Preparation, application and testing of permanent antibacterial and antiviral coatings. *Nature Protocols, 2,* 2412-2417.

11. Haldar, J., An, D., Alvarez de Cienfuegos, L., Chen, J., & Klibanov, A.M. (2006). Polymeric coatings that inactivate both influenza virus and pathogenic bacteria. *Proc. Natl. Acad. Sci. USA, 103,* 17667-17671.

12. Ryan, M.E., Hynes, A.M., & Badyal, J.P.S. (1996). Pulsed plasma polymerization of maleic anhydride. *Chem. Mater., 8*, 37-42.

13. Han, L.M., Rajeshwar, K., & Timmons, R.B. (1997). Film chemistry control and electrochemical properties of pulsed plasma polymerized ferrocene and vinylferrocene. *Langmuir, 13*, 5941- 5950.

14. Briggs, D. (1998). Surface Analysis of Polymers by XPS and Static SIMS, Cambridge University Press, NY.

15. Pels, J.R., Kapteijn, F., Mouljn, J.A., Zhu, Q., & Thomas, K.M. (1995). Evolution of nitrogen functionalities in carbonaceous materials during pyrolysis. *Carbon*, 33, 1641-1653.

16. Li, J., Qian, X., Wang, L., & An, X. (2010). Polyaniline-coated conductive paper. *BioResources*, 5, 712-726.

Biocompatibility and Biofilm Inhibition of *N, N*-hexyl, methyl-polyethylenimine Bonded to Boston Keratoprosthesis Artificial Cornea

INTRODUCTION

Indwelling prosthetic devices have been critical in saving numerous lives and enhanced the quality of life for even more patients. Yet the presence of an indwelling foreign body both predisposes to, and complicates the eradication of, infections, often with biofilm formation. Device-related biofilm infections account for an estimated 60% of all hospital-associated infections [14] and add $5 billion per year to U.S hospital costs [8]. Biofilms, heterogenous collections of bacteria encased by a secreted matrix called extracellular polymeric substance (EPS) [28], adhere strongly to surfaces, are resistant to antimicrobials and other biocides, and are protected from host immune defenses. The risk of a biofilm-associated medical device infection depends on its location with any implantable device that translocates from the surface of the body (skin, cornea) into a sterile body site (blood, urine, intraocular) being particularly at greater risk [1,2].

The Boston Keratoprosthesis (B-KPro) is an artificial cornea that is a treatment option for corneal disorders not amenable to standard penetrating keratoplasty (corneal transplantation). The B-KPro has the shape of a collar button and consists of a transparent medical-grade poly(methyl methylacrylate) (PMMA) front plate with a stem, that houses the optical portion of the device, and a back plate with holes composed of either PMMA or medical-grade titanium. During implantation, the device is assembled with a donor corneal graft positioned between the front and back plates with extension of the optic stem into the anterior chamber of the eye; a titanium C-ring locks the assembly (Figs. 1A, B, C) [3]. Its postoperative management includes the continuous wearing of a soft contact lens to prevent ocular surface dehydration and tissue melt [4]. Daily low-dose topical antibiotic prophylaxis is required [5], as well as low-dose topical steroids in many patients [6]. While the use of life-long daily antibiotic prophylaxis to prevent infection has been effective, long-term medication adherence and emergence of resistant organisms continue to be concerns, especially in the developing world [*Ref.*].

Thus there is a need for keratoprostheses and other implantable medical devices that inherently resist bacterial infection long-term. Most biocidal products depend on a timed release of antibiotics, heavy metal ions (notably silver), or other biocides. Once all the biocide has been released, the antimicrobial activity ends, leaving foreign material *in situ*; consequently, the overall benefit of antibiotic-impregnated materials remains unclear [7]. Given the large health care costs of medical-device and hospital-acquired infections [8], materials that effectively and permanently limit microbial adherence and viability and are themselves non-toxic is badly needed.

It would be most desirable to permanently attach coatings onto PMMA and other currently used prosthetic materials that either prevent adherence of bacteria or kill them on contact, thereby inhibiting the formation of biofilms. Recently, non-leaching, long-chained hydrophobic polycations that can be attached covalently to the materials' surfaces and render them strongly antimicrobial have been developed [22B,32]. Specifically, immobilized *N,N*-

hexyl,methyl-polyethylenimine (HMPEI) (Figure 1D) has broad antibacterial and antiviral properties [9-12].

We report herein *in vitro* assessments of HMPEI attached to PMMA and titanium materials used in the construction of the B-KPro. Antimicrobial efficacy using hyperbiofilm-forming clinical isolates of *Staphylococcus aureus*, as well as *in vitro* cell cytotoxicity using immortalized human corneal epithelial cells, were investigated. *In vivo* biocompatibility studies with new ocular models in the rabbit comparing HMPEI-derivatized and parent PMMA and titanium, as well as the Boston K-Pro with applicability to other implantable medical devices, were examined. Evaluation of biocompatibility was by clinical assessment, histopathology, and scanning electron microscopy looking for toxicity or abnormal host responses.

2. MATERIALS AND METHODS

2.1 Materials

Laboratory chemicals, branched PEI [12], and organic solvents were from Sigma-Aldrich Chemical Co. (St. Louis, MO).

The Boston Keratoprosthesis (B-KPro) parent materials were medical-grade poly(methyl methacrylate) (PMMA) (Spartech Townsend, Pleasant Hill, IA) and titanium 6-4 ELI (Ti) (Dynamet, Washington, PA) processed by J.G. Machine Co. (Woburn, MA). PMMA discs were cut from a 1-cm rotating PMMA rod in 200- and 150-micron thickness. Smaller PMMA discs (3, 1.5, and 1.0 mm) were punched out using Micro Punch Set (Micro-Mark, www.micromark.com). Titanium discs (10, 3.0, and 1.0 mm in diameter) were punched biopsied from a single Ti sheet (150 micron thickness). KPro Front Pieces (KPro-FP) were made of either a large (KPro-FP-L) 4.75 mm front plate diameter and 3.3 mm stem diameter or a smaller (KPro-FP-S) 2.7 mm front plate diameter and 1.5 mm stem diameter; all had a 2 mm stem length. Boston Keratoprosthesis Type I (B-KPro), threaded design (pseudophakic) had a front plate diameter 5.0 mm and a stem diameter 3.35 mm. The PMMA threaded back plate had a diameter of 8.5 mm, plate thickness of 0.8 mm, and 16 holes of 1.2 mm diameter each.

Povidone-iodine ophthalmic solution 5% (Betadine 5%™, Alcon, Fort Worth, TX) was the preoperative antiseptic. Ciprofloxacin powder was from Sigma-Aldrich. Ciprofloxacin HCl ophthalmic solution 0.3% (Sigma-Aldrich), polymyxin B (10,000 polymyxin B U/mL and 1 mg trimethoprim sulfate) ophthalmic solution USP with benzalkonium chloride 0.004% preservative (Bausch & Lomb, Tampa, FL), prednisolone acetate ophthalmic solution 1% (Falcon Pharmaceuticals (Alcon), Fort Worth, TX), and triamcinolone acetonide injectable suspension USP 40 mg/mL (Kenalog-40™, Bristol-Myers-Squibb, Princeton, NJ) were obtained from the MEEI Pharmacy. Balanced salts solutions (BSS™ and BSS Plus™, Alcon) were used for ocular irrigation. Xylazine injectable solution 100 mg/mL (Tranquived, Vedco, St. Joseph, MO), ketamine HCl USP 100 mg/mL (Ketaject™, Phoenix Pharm, St. Joseph, MO), and proparacaine HCl ophthalmic solution USP 0.5% (Bausch & Lomb) were used as anesthetic agents. Pentobarbital solution 390 mg/mL (Fatal-Plus, Vortech Pharm, Dearborn, MI) was used for euthanasia.

The surgical dissecting instruments were Super Sharp Blade, 30 degree, 3.5 mm (K-blade, Katena Products, Denville, NJ), crescent microsurgical knife 2.0 mm angled, bevel up blade (Katena Products), Graefe micro dissecting knife, 0.5 mm tip diam. (Fine Science Tools, Vancouver, British Columbia, Canada), trephine 8.5mm (Storz Instr., Bausch & Lomb), and 3 mm and 1.5 mm biopsy punches (Acu-Punch, Acuderm, Ft. Lauderdale, FL). Black monofilament nylon (Ethilon™ 10-0 and 8-0) and coated polyglactin 910 (Vicryl™ undyed braided 6-0) were used for suturing (Ethicon (Johnson & Johnson), Somerville, NJ). Intrastromal injections were with a custom-made chromatography microliter glass syringe with a 33 gauge, 30 degree beveled needle (Hamilton Co., Reno, NV).

2.2 Strains and Media

Since *Staphylococcus aureus* is a normal commensal on the skin and ocular surface, yet infection (including device-associated biofilm infections [14]) appears to be predominantly caused by a subset of organisms that possess certain microbiologic virulence traits (29-31), we first screened *S. aureus* clinical isolates that caused infection for their ability to form biofilm. In addition, since previous reports have indicated the influence of media composition on *in vitro* biofilm production, we evaluated our clinical isolates for biofilm production under various media and growth conditions (Table 1).

Fourteen *S. aureus* clinical isolates, including methicillin-sensitive (9) and methicillin-resistant (5) ones, were obtained from the Massachusetts Eye and Ear Infirmary (MEEI) Porter Bacteriology Laboratory [15]. These isolates were frozen within two passages to minimize loss of *in vivo* virulence from representative eye, skin, and mucous membrane infections. Three *S. aureus* laboratory strains (gift of Dr. G. Pier, Channing Lab, Boston, MA) [16] served as biofilm controls: MN8 [17], a toxic shock syndrome clinical isolate, that produces moderate amount of biofilm; MN8 mucoid (MN8m), a spontaneous mutant isolated from a chemostat culture of MN8 that constitutively overproduces the polysaccharide intercellular adhesion (poly-N-acetyl-1,6 glucosamine (PNAG)), a hyperbiofilm strain; and an isogenic mutant, MN8m□*ica::tet,* containing a deletion in the *ica* locus which impairs biofilm formation. The minimal inhibitory concentration (MIC) was determined on planktonic bacteria by Clinical Standards and Laboratory Institute methods [18]. Strains were evaluated for biofilm production in three different antibiotic-free media (brain heart infusion (BHI), trypticase soy broth (TSB), and Luria-Bertani (LB)) with various carbohydrate sources (glucose and sucrose) and concentrations, and at different time points.

2.3 Material Modification Syntheses

Materials and Methods:

The covalent modification of the PMMA and the titanium were done as shown below.

Schematic representation of modification of PMMA discs:

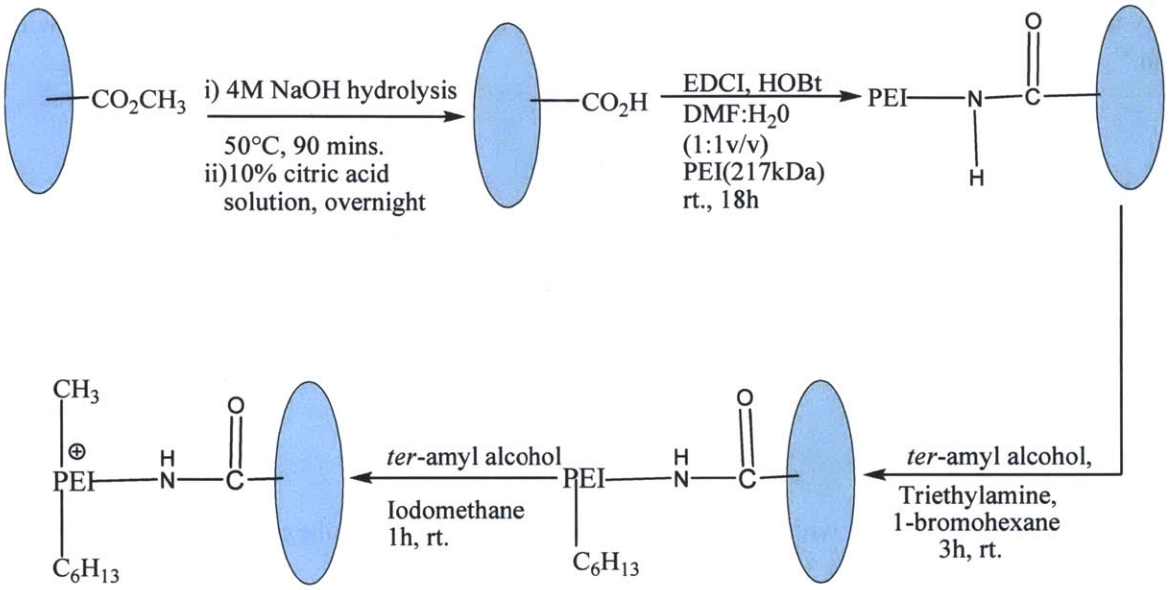

EDCI = (3-(Dimethylamino)propyl)ethyl carbodiimide hydrochloride
HOBt= 1-Hydroxybenzotriazole
PEI = Poly(Ethyleneimine)

Step 1: PMMA discs (120 numbers) were treated with 15ml (4M) NaOH at 50°C for 90 minutes. The discs were taken out and were immersed in 10% citric acid solution (15ml) overnight. The discs were washed repeatedly with deionized water until the pH of the reach neutral pH. The discs were dried in air.

Step 2: The PMMA discs (120 numbers) after hydrolysis reaction were treated with a 1:1 solution of DMF/water (total volume 32 ml) containing 1.2gms of linear polyethylenimine, 4.5 grams of 1-Hydroxybenzotriazole and 4.5gms of (3-(Dimethylamino)propyl)ethyl carbodiimide hydrochloride. The reaction was carried out overnight at room temperature overnight for 18 hours. After the completion of the reaction, the discs were thoroughly washed with deionised water and dried in air.

Step 3: PMMA discs (60 numbers) obtained form the previous reaction was treated with 6ml 1-bromo hexane, 6ml of triethylamine and 3.5ml of tertiary amyl alcohol as the solvent. The reaction was carried out at room temperature for 3 hours.

Step 4: 12 discs were treated with 500 µl of *ter*-amyl alcohol and 500µl of iodomethane for 1 hour. The discs after the reaction were put into water and then washed with methanol.

To quantify the polymer on the surface of the PMMA discs we titrated quaternary ammonium group with fluorescein.[11]

PMMA backplate and screw:

PMMA back plates and screw were immersed in fresh 4M NaOH solution (2.2 ml), 50°C for 90 mins.

Back plate and screw was treated with 300 mg LPEI, 800 mg of HOBt (2.5 ml DMF) and 800 mg of EDCI (2.5 ml water) in a total volume of 5ml of DMF and water (1:1 vol/vol) at room temperature. They were then washed with water.

Back plate and screw were treated with 1.5 ml triethylamine, 1.5 ml 1-bromohexane and 750 µl of *ter*-amyl alcohol at room temperature for 3 hours.

Back plate and screw was treated with 750 µl of iodomethane and 750 µl of *ter*-amyl alcohol for 1hour and 15 mins at room temperature for 1 hour. The discs were then washed with water and methanol.

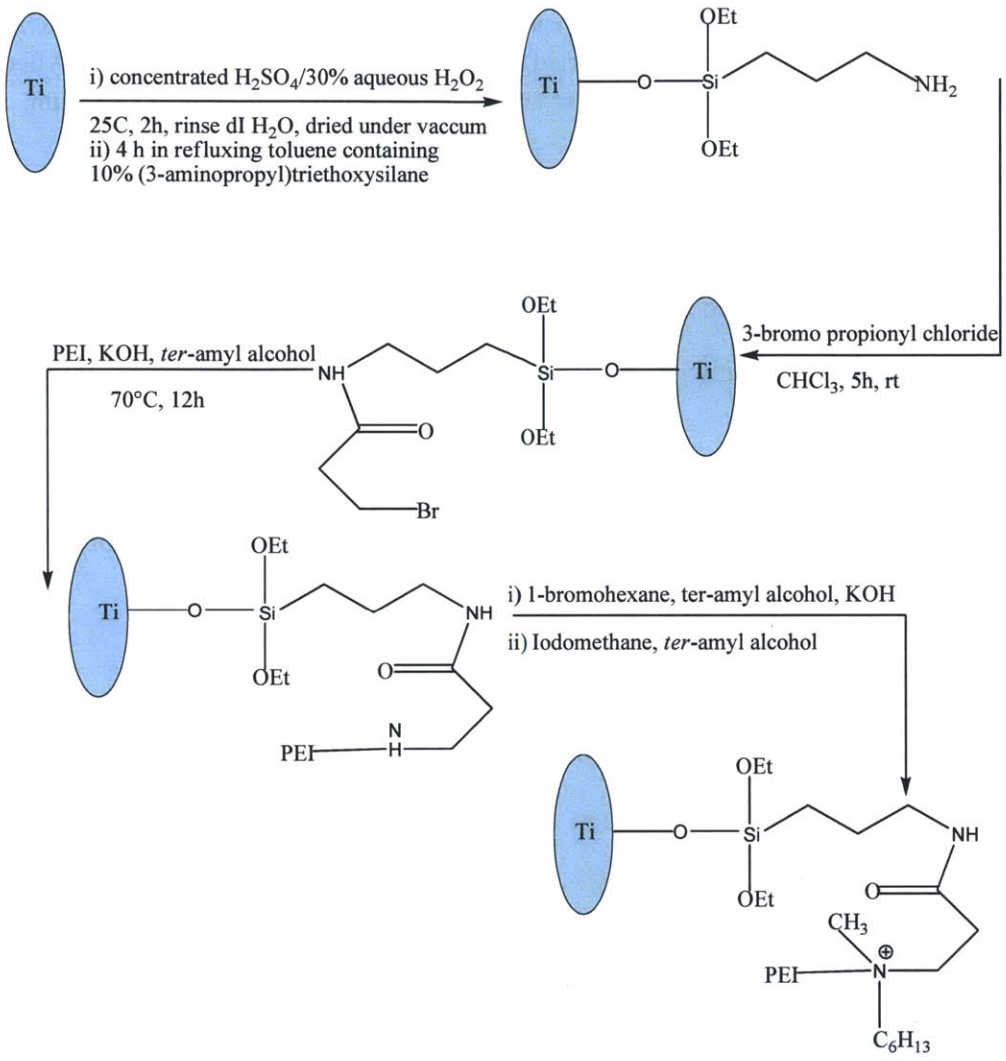

Step 1: Samples[20] were rinsed with toluene and then treated at 25°C for 2 h with a solution consisting of equal volumes of concentrated H_2SO_4 and 30% aqueous H_2O_2. The cleaned, oxidized samples were then rinsed with distilled water and dried under vacuum.

Step 2: Silanization[20] of oxidized samples (17 titanium discs) was performed by heating them for 4 h in refluxing toluene containing 10% (3-aminopropyl)triethoxysilane, after which they were rinsed with toluene and dried under vacuum.

Step 3: The silanized titanium discs (14 in number) were treated with 4-bromobutyryl chloride for 5 hours in chloroform at room temperature. After the reaction the discs were washed with chloroform to remove any excess 4-bromobutyryl chloride.

Step 4. The discs from step 3 were treated with 1gram linear polyethylenimine, 90 milligrams of KOH and 10 ml of tertiary-amyl alcohol. The reaction was carried out by heating at 70°C for 12 hours. After completion of the reaction the discs were washed with water and methanol and then dried under vacuum.

Step 5 (i) The discs from step 4 were treated with 1-bromohexane (1.2 ml) , tertiary-amyl alcohol (8 ml) and potassium hydroxide (90 mg)at room temperature. After the completion of the reaction the discs were washed with water and methanol and then dried under vacuum.

(ii) The treated discs were finally quarternised with 1ml of iodomethane and 4 ml of tertiary-amyl alcohol.

DMPEI (N,N-dodecyl,methyl PEI) linear and branched were synthesized as previously described [1] and the PMMA discs were painted with the solution of the polymers in on both sides more than once to make sure that the disc is uniformly coated

2.4 Cleaning and Sterilization Methods

All materials were washed in a mild detergent with ultrasonic bath cleaning, rinsed extensively with distilled water, and ethanol dried. Materials were sterilized by ethylene oxide at 37°C.

2.5 Confocal Scanning Light Microscopy

To assess *in vitro S. aureus* biofilm formation and adherence, overnight cultures were grown from a freshly streaked single colony in BHI-2% sucrose, back diluted 100-fold, and aliquoted onto 1-cm sterile discs (HMPEI-PMMA and PMMA; HMPEI-Ti and Ti) in 24-well cell culture dishes for 24 h and 6 days under static growth conditions at 37°C.

Samples were washed with 0.9% NaCl, stained with acridine orange, and affixed to a small clear plastic Petri dish. Samples were examined using a Leica TCS-SP2 confocal scanner connected to an inverted microscope (Leica Microsystems, Heidelberg, Germany). For 100X oil-immersion objective, 0.9% NaCl was added to the Petri dish. 3-D confocal images and sequential scans at 488 and 568 nm were obtained. Due to the autofluorescence of HMPEI coated-materials, a third channel, at 633 nm, was added. One-micron sequential scans were obtained from four predetermined representative areas. These experiments were performed in triplicate on separate days.

2.6 Field Emission Scanning Electron Microscopy

In vitro S. aureus biofilm samples were grown similarly as described in the preceding section. Both *in vitro* and *in vivo* samples were fixed with ½ strength Karnovsky's solution, dehydrated through graded ethanols, critical-point dried (Autosamdri 795 Supercritical Point Dryer, Tousimis, Rockville, MD), and mounted and sputter coated with chromium (Model 681 Ion Beam Coater, Gatan, Pleasanton, CA). The entire surface of each specimen was examined

with a field emission scanning electron microscope (JEOL 7401F; JEOL, Tokyo, Japan).

2.7 *In vitro* Biofilm Analysis of *S. aureus* Isolates

S. aureus clinical isolates from MEEI Clinical Laboratory and two laboratory biofilm-positive and –negative strains were screened for biofilm formation by a static microtiter plate biomass assay using a Gentian violet stain as described [19]. Overnight *S. aureus* cultures were diluted (1% vol/vol) in non-selective media with various carbohydrate sources and aliquoted into 96-well polystyrene flat-bottomed microtiter plates at 0.2 ml per well (Corning Life Sciences, Corning, NY). After 24, 48 or 96 h without shaking at 37°C, the wells were washed three times with phosphate-buffered saline (PBS) and stained with Gentian violet. Eluted crystal violet absorbance at OD_{595} was measured by spectrophotometry (Tecan GENios microplate reader, Phoenix Research Products, Research Triangle Park, N.C.). Experiment was performed in triplicate and repeated three times, the data was then averaged and standard deviation was calculated. The mean OD value obtained from media control well was deducted from all the test OD values. A representative biofilm robustness grading system was assigned to each strain under different growth conditions (Table 1).

2.8 Screening Different PEI Variants for *S. aureus* Biofilm Formation Inhibition

DMPEI branched and linear variants [9, 12] applied to PMMA were compared using the aforementioned representative robust biofilm-forming ocular isolates and *S. aureus* biofilm laboratory strains. Cultures were grown as above in BHI with 2% sucrose, diluted 100 fold, and 1 ml was aliquoted into 24-well tissue culture plates (Corning Life Sciences) with each well containing a 1-cm disc. Plates were incubated overnight without shaking at 37°C and biomass measured by Gentian violet staining assay.

2.9 *In vitro* Human Corneal Epithelial Cell Cytotoxicity Assays

Telomerase-immortalized human corneal-limbal epithelial (HCLE) cells were obtained from Dr. I. Gipson (Schepens Eye Research Institute, Boston, MA), plated at 2 $x10^4$ cells/cm^2 in 24-well tissue culture plates (Laboratory-Tek, Naperville, IL) in keratinocyte serum-free medium (K-SFM; Invitrogen-GIBCO, Carlsbad, CA) at 37°C in a 5% CO_2 [20] After stratification of the corneal cells [20] 1-cm^2 PMMA and HMPEI-PMMA discs were placed on the apical epithelial cells, and their cell surface damage was assessed with rose bengal staining [20]. Morphological and cytotoxicity experiments were performed in triplicate on three separate days. Phase contrast morphological assessment was with an inverted light microscope (Eclipse TS100/100-F Nikon, Tokyo, Japan). Micrographs were taken with a digital camera (SPOT Insight Fire Wire; Diagnostic Instruments, Sterling Heights, MI). Quantitative assessment of cell cytotoxicity was performed measuring the cytosolic enzyme lactate dehydrogenase (LDH) released upon lyses of HCLE cells (CytoTox96™, Promega, Madison, WI); absorbances at 490 nm were measured. Experiments were performed in triplicate on three separate days.

2.10 Optical Testing

To assess for any optical changes to the B-KPro Type I, both uncoated and coated devices were assessed. The B-KPro was clamped in a black iris diaphragm mounted on the rail of an optical bench containing a 3X and a 10X objectives. The microscope was moved vis-à-vis the B-KPro until the illuminated Snellen's chart positioned at 20 ft became sharply focused.

2.11 *In vivo* Toxicity Studies

2.11.1 Animals

All animals used in this study were treated in accordance with the Association for Research in Vision and Ophthalmology (ARVO) Statement for the Use of Animals in Ophthalmic and Vision Research and were approved by the Massachusetts Eye and Ear Infirmary Institutional Animal Care and Use Committee (Boston, MA). Only one eye per animal was used. The New Zealand white rabbits (Millbrook Farm Breeding Lab, Amherst, MA) weighed between 3.5 and 5.0 kg were anesthetized with intramuscular injection of ketamine HCl (35 mg/kg) and xylazine HCl (10 mg/kg). The BALB/c mice were 20-30 grams (Charles River Laboratories, Wilmington, MA) and received a combination xylazine/ketamine mixture intraperitoneally (50 mg/kg).

2.11.2 Surgical procedures

Anesthesia was given 15 min prior to surgery. Topical proparacaine HCl 0.5% was instilled into the conjunctival sac of the eye, and the operating area was sterilized with 5% povidine-iodine and repeated after 5 min. Topical ophthalmic antibiotics (Polytrim™) were given immediately pre-operatively. Animals were placed in a laterally recumbent position for surgery.

2.11.3 Clinical assessment and photography

Clinical assessment was performed by two independent observers and the following parameters [21] were assessed: 1) corneal haze/infiltrate, 2) corneal edema, 3) corneal neovascularization, 4) conjunctival irritation/chemosis, 5) conjunctival discharge, 6) epithelial abnormalities, 7) anterior chamber cells and/or flare, 8) iritis +/- pupil size, 9) retroprosthetic membranes, and 10) cataract formation. Parameters 1-6 were evaluated for all clinical examinations, while those 7–10 were additionally evaluated by slit lamp biomicroscopy. These were graded on a scale of 0 (absent) to 4 (most severe) in relationship to the materials used and potential confounders (surgical wound and sutures) with a theoretical maximum of 40 (Table 2).

Photography was performed using Nikon D90 digital single-lens reflex (SLR) camera attached either to a Zeiss digital SLR camera adapter for the Zeiss OPMI Lumera/S7 ophthalmic

surgical microscope (Carl Zeiss Surgical GmbH, Oberkochen, Germany) or directly to Topcon slit lamp microscope (Kogaku Kikai K.K., Tokyo, Japan).

2.11.4 Histological examination

Immediately after euthanasia, eyes were enucleated and fixed in neutral buffered formalin, dehydrated, embedded in paraffin, sectioned, and stained with hematoxylin and eosin.

2.11.5 Intrastromal disc reactivity model

In the BALB/c mice, a cornea incision was made with a Super Sharp blade, and a lamellar corneal micropocket was created using a Graefe microdissecting knife. Either PMMA or HMPEI-PMMA 1-mm discs were placed intrastromally in one eye of each animal. The corneal wound was closed with one 10-0 nylon suture in the earlier pilot experiments. In subsequent experiments, the corneal wound was left unsutured. A partial tarsorrhaphy with one 8-0 suture was performed on all animals. One dose of antibiotics pre-operatively and and immediately postoperatively were given. No post-operative antibiotics or topical steroids were administered. (n = 4 groups)

In the New Zealand white rabbit, a cornea incision in the periphery of the cornea was made with a Super Sharp blade. A lamellar corneal micropocket was tunneled to the corneal center using a 2.0-mm angled, bevel-up crescent microsurgical knife. Comparative parent PMMA or HMPEI-PMMA discs of 3.0 and 1.5 mm in diameter, or parent Ti 6-4 ELI or HMPEI-Ti 6-4 ELI discs (3.0 mm in diameter) were placed intrastromally in one eye of each animal. The corneal wound was closed with two 10-0 nylon sutures in the earlier pilot experiments. In subsequent experiments, the corneal wound was left unsutured with lengthening of the corneal tunnel pocket. A partial tarsorrhaphy with three 6-0 sutures was performed on all animals and removed by the third day. One dose of polymyxinB/trimethoprim pre-operatively, immediately postoperatively, and daily for two subsequent postoperative days was given. No steroids were given. (3 mm discs, n = 4 groups; 1.5 mm discs, n = 3 groups)

2.11.6 Anterior chamber disc reactivity model in the rabbit

A corneal incision was made through the cornea into the anterior chamber using a Super Sharp blade. PMMA and HMPEI-PMMA discs, 3 mm in diameter, were placed into the anterior chamber. The corneal wound was closed with two 10-0 nylon sutures and removed within one week. Immediately post-operatively and daily for two subsequent days, topical antibiotic polymyxinB/trimethoprim ophthalmic solution and a topical steroid, prednisolone acetate 1% ophthalmic suspension, were given. (n = 1 set)

2.11.7 Keratoprosthesis front piece intrastromal-anterior chamber reactivity model in the rabbit.

To assess reactivity in the two major eye compartments, corneal stroma and anterior chamber, that the B-KPro resides in and to enable evaluation in the anterior chamber without floating or uncontrolled attachment to adjacent tissues, we developed a two-compartment eye model using differently sized KPro front pieces, KPro-FP-L (4.75 mm front plate/3.3 mm stem diameter) and KPro-FP-S (2.7 mm front plate/1.5 mm stem diameter). The rabbit's cornea was dissected vertically to 50% depth using a Super Sharp blade. A corneal lamellar dissection was performed to create a semi-circle area. The cornea was flapped over but remained attached and either a 3.0 mm or a 1.5 mm trephine opening was made centrally in the dissected cornea. The front plate was placed at 50% depth in the dissected corneal stroma with extension of the stem into the anterior chamber of the rabbit's eye. The corneal flap was pulled over the KPro front piece and sutured in place using six 10-0 nylon sutures. Immediately post-operatively and daily for two subsequent days, both topical antibiotic polymyxinB/trimethoprim ophthalmic solution and a topical steroid, prednisolone acetate 1% ophthalmic suspension, were given (KPro-FP-L, n = 1 set; KProFP-S, n = 2 sets).

2.11.8 B-KPro Type I with a corneal autograft reactivity model in the rabbit

The rabbit's cornea was cut with a 8.5 mm trephine blade and excision of the corneal button was with corneal scissors. The autograft cornea was placed in a Teflon well, and a 3.0 mm trephine opening was made with an Acu-Punch centrally. The keratoprosthesis front part was placed upside-down, the corneal graft was slid over the stem, and the backplate was positioned over the stem and lightly screwed on until resistance was met. Viscoelastics and the titanium C-locking ring were not used as in routine B-KPro surgeries to avoid confounding material variables. Finally, the graft with its prosthesis was placed in the trephine opening. The surgical wound was closed with 12 interrupted 10-0 black monofilament nylon sutures equally spaced, and the knots were buried. PolymyxinB/trimethoprim drops but no steroids had been given during the procedure, and no contact lens was placed. A lateral partial tarsorrhaphy using three interrupted 6-0 coated Vicryl sutures were placed and removed within three days. Immediately post-operatively and daily until one week prior to the end of the experiment, topical antibiotic polymyxinB/trimethoprim ophthalmic solution was given. A topical steroid, prednisolone acetate 1% ophthalmic suspension, was given immediately post-operatively and daily for one month in the pilot PMMA B-KPro only experiment and daily for 7 post-operative days in the HMPEI-PMMA compared to PMMA experiment (PMMA B-KPRo, n = 2; HMPEI-PMMA B-KPro, n = 1).

3. RESULTS

3.1 *In vitro* Studies

3.1.1 Selection of ocular-associated clinical isolates of *S. aureus* for biofilm formation with different *in vitro* media

Given our hypothesis that infection is caused by a subset of organisms that possess microbiologic virulence traits [29-31] and due to previous reports indicating the influence of media composition on *in vitro* biofilm production[*Ref*], we evaluated *S. aureus* laboratory strains and clinical isolates for biofilm production under various media and growth conditions (Table 1). As others[*Ref*], we found our *S. aureus* strains formed biofilms variably under different conditions. We selected those ocular-associated strains that formed robust biofilms under diverse *in vitro* media and growth conditions (Table 1) for further studies. Our hyperbiofilm laboratory mutant, MN8m, did prove to avidly self-adhere but its adherence to polystyrene was variable under different growth conditions. Since our ocular and mucosal surface isolates formed biofilms most robustly with BHI-2% sucrose, it was used for subsequent studies.

3.1.2 Screening of *N*-alkyl-PEI derivatives with selected *S. aureus* biofilm strains

We screened both branched and linear versions of various lengths of DMPEI painted on PMMA with selected clinical ocular isolates of *S. aureus* and MN8m [16] for biofilm formation inhibition. Linear, 217-kDa DMPEI attached to PMMA exhibited the greatest inhibition of *S. aureus* biofilm formation; moreover, longer alkyl chain lengths beyond C_6 conferred no significant benefit, as shown previously [12]. Unfortunately, DMPEI painted on the surface of PMMA chipped under our biofilm growth conditions. Therefore, in all subsequent experiments HMPEI covalently attached to PMMA and titanium was employed.

3.1.3 Confocal scanning light microscopy (CSLM) of *in vitro S. aureus* biofilms

Three ocular-associated *S. aureus* isolates (MEEI-IB001, -012, -013), a hyperbiofilm strain (MN8m), and a defective biofilm strain (MN8m□*ica::tet)* were grown on both HMPEI-coated and parent materials (PMMA and Ti; 1-cm discs) *in vitro* for 24 h and 6 days. As seen for HMPEI-PMMA and PMMA in Figs. 2A and 2B (similar data for titanium not shown), significant inhibition of bacterial biofilms in all clinical isolates was revealed by confocal scanning light microscopy. There was over 99% inhibition of both the laboratory-derived MN8m [22B] and the defective biofilm MN8m(□) strains.

Due to the autofluorescence of acridine orange stained HMPEI coated-materials, a third channel was added (633 nm, Cy6-blue) for qualitative assessment. An accurate quantitative measurement of biofilm biomass thickness and height was limited by: 1) the focal length available to measure mature biofilms grown on 150-200 micron thickness discs within a tissue culture dish and 2) the autoflourescence of HMPEI itself. There was at least a 4- to 8-fold inhibition in *S. aureus* biofilm thickness on HMPEI-PMMA (Fig. 2A) compared to that on parent PMMA (Fig. 2B) *in vitro*. There was likewise a 2- to 4-fold less biofilm formation on HMPEI-Ti materials compared to that on parent Ti *in vitro* (data not shown) (note that our *S. aureus* strains preferentially grew biofilms on parent PMMA compared to parent Ti).

3.1.4 Scanning electron microscopy (SEM) of *in vitro S. aureus* biofilms

Biofilm formation and adherence by three ocular-associated *S. aureus* isolates (MEEI-IB001, -012, -013), a hyperbiofilm strain (MN8m), and a MN8m□□*ica::tet* defective biofilm

grown on HMPEI-PMMA discs compared to those on unmodified PMMA discs were examined by SEM. The inhibition of biofilm formation persisted in all *S. aureus* isolates after 6 days of continuous static growth on HMPEI-PMMA (Fig. 2C), while the bacteria grown on parent PMMA continued to accumulate more mature biofilm structures (Fig 2D). In addition, lysis of bacterial cell walls resulting in sickled shaped cells was observed on HMPEI-PMMA discs (Fig. 2C). The hyperbiofilm strain (Fig 2E) and the defective biofilm strain showed over 99% biofilm inhibition when grown on HMPEI-PMMA discs compared to unmodified PMMA discs. The only bacteria that remained intact were seen suspended on a bacterial-derived extrapolysaccharide matrix (EPS) and not in contact with the coated HMPEI-PMMA material below (Fig 2E).

3.1.5 *In vitro* cytotoxicity studies

To screen for cytotoxicity *in vitro*, HMPEI-PMMA discs were compared to parent PMMA counterparts by placing them on confluent immortalized human corneal limbal epithelial (HCLE) cells. HMPEI-PMMA appears to exhibit no additional toxicity (Fig. 3A) in comparison to PMMA (Fig. 3B) on HCLE cells. Similar morphological disruption of the stratified HCLE cells after placement of unadhered discs was seen in both HMPEI-PMMA and parent PMMA discs after the first 48 h, and similar epithelial cell growth and recovery was seen on HMPEI-PMMA and PMMA discs by 72 h (Figs. 3A and 3B). Rose bengal staining demonstrated equal stratification of HCLE cells grown on HMPEI-PMMA and PMMA discs (data not shown).

Quantitative assessment of lysed HCLE cells by a lactate dehydrogenase (LDH) release cell cytotoxicity assay showed no additional cell cytotoxicity in the case of HMPEI-PMMA discs compared to PMMA ones at 24 h, and there was statistically significantly less cytotoxicity seen on HMPEI-PMMA discs compared to the control PMMA ones by 48 and 72 h (p values < 0.0001 and <0.01, respectively). These results are consistent with the lack of HMPEI-associated mammalian cell cytotoxicity seen in monkey kidney cells reported previously [9].

3.1.6 Optical properties of the Boston Keratoprosthesis with HMPEI covalent modification

Covalent attachment of HMPEI to Boston Keratoprostheses did not alter its optical clarity or its refractive optical power.

3.2 *In vivo* Evaluation

3.2.1 Intrastromal disc reactivity model

Since the B-KPro is predominantly in contact with the corneal stroma, this model was designed to evaluate for any toxicity seen within the corneal stroma of the rabbit (Fig. 4A). There was less corneal inflammatory response with HMPEI-PMMA discs compared to PMMA ones in both BALB/c mice (data not shown; N = 4 for 1 mm Discs) and New Zealand white

rabbits (Fig. 5; N = 4 for 3 mm PMMA discs; N = 3 for 1.5 mm PMMA discs). There was also less corneal edema, corneal haze, neovascularization, and conjunctival irritation and discharge seen with HMPEI-PMMA 3 mm discs (Fig. 5A) compared to PMMA 3 mm ones (Fig. 5B) intrastromally (Table 2). Histopathology demonstrated that intrastromal HMPEI-PMMA discs showed no more inflammation than unmodified PMMA ones (data not shown), whether they were surgically removed or spontaneously extruded.

HMPEI-Titanium (Ti) discs (Fig. 5C; N = 4) when compared to parent Ti ones (Fig. 5D; N = 4) demonstrated no more reactivity by clinical assessment. The histopathologic examination of the titanium discs showed an excellent host stromal tolerance with both coating of HMPEI (Fig8A; 61 days) and without coating (Fig 8B; 61 days). There was no evidence of inflammation, vascularization, or active scar formation (Fig 8, A and B). Scanning electron microscopy of the HMPEI-Ti discs (Fig. 9A – 25X, inset 500X; 61 day) and parent Ti discs (Fig. 9B – 25X, inset 500X; 61 days) extracted from the corneal stroma at 37 days and 61 days revealed no inflammatory response to either. In addition, denser, more compact and confluent cells were seen on HMPEI-Ti discs (Fig. 9A) than on parent Ti discs (Fig. 9B).

3.2.2 Anterior chamber disc reactivity model

HMPEI-PMMA discs were no more reactive than the parent PMMA ones when placed in the anterior chamber of the eye. Although the reactivity was greater in the anterior chamber model than in the intrastromal model (data not shown), the unpredictable free-floating movement of the discs within the anterior chamber limited this model's usefulness.

3.2.3 Intrastromal-anterior chamber reactivity model

Using a Keratoprosthesis front piece (KPro-FP) placed with the front plate into the corneal stroma and the stem extending into the anterior chamber (Fig. 4B), the reactivity in the rabbit was assessed over time. On post-operative day 2, HMPEI-PMMA KPro-FP (Fig. 6A) appeared similar to PMMA KPro-FP (Fig. 6B) with the exception of the onset of iritis in PMMA KPro-FP. There was less corneal edema, haze, neovascularization, conical ectasia, and conjunctival discharge in HMPEI-PMMA KPro-FP (Fig. 6C) compared to parent PMMA KPro-FP (Fig. 10D) by post-operative day 30. By three months, these changes progressed further in the PMMA KPro-FP (Fig. 10F, Table 2), while the HMPEI-PMMA KPro-FP remained relatively unchanged (Fig. 10E, Table 2). Small retroprosthetic membranes formed on both PMMA and HMPEI-PMMA stems. Front pieces were surgically extracted on post-operative day 105. The histopathologic examination of PMMA front pieces with and without HMPEI coating disclosed that there were different host stromal responses. The HMPEI-coated specimen showed a fibroblast reparation response surrounding the posterior aspect of the implant front piece without inflammation or vascularization (Fig. 8C). The non-coated front piece displayed moderate acute inflammation with minimal microvascularization (Fig. 8D). SEM showed denser, more compact and confluent cells attached to HMPEI KPro-FP (Fig. 9C) compared to looser, disorganized cells attached to the control PMMA KPro-FP (Fig. 9D).

3.2.4 B-KPro Type I with corneal autograft reactivity model in the rabbit

To assess the effect that the HMPEI coating may have on all the parts of the eye (epithelial layer, stroma, endothelium, anterior chamber, and the corneal graft healing), a human sized B-KPro Type I with a corneal autograft was placed with less topical steroid usage. When HMPEI-PMMA B-KPro (Figs. 7A, 7C) is compared to the uncoated PMMA B-KPro at postoperative day 69 (Figs. 7B, 7D) in the rabbit, less corneal edema, haze, and conjunctival discharge is observed (Table 2). As seen with the KPro-FP model on the side view, the control PMMA B-KPro underwent conical ectasia of the cornea (Fig. 9D) that was not observed in the HMPEI B-KPro in the rabbit. This conical reshaping of the cornea is unique to the rabbit and not seen in humans with a B-KPro. In addition, epithelial growth on the front piece was seen with HMPEI-PMMA B-KPro (Figs. 7A, 7C), while it did not occur on control PMMA B-KPro surfaces (Figs. 7B, 7D) in the rabbit (nor does it occur normally on PMMA front piece surfaces in humans [25]). Even with mechanical removal of the epithelial growth, the epithelium re-grew within one month.

DISCUSSION

HMPEI exerts its antimicrobial effects by long hydrophobic polycationic chains that are permanently attached to various materials and are able to penetrate and lyse the cell wall of microorganisms [22B, 32]. This contact-dependent killing has been demonstrated for viruses, planktonic bacteria, and yeast [10-12], but up till now not for bacterial biofilms that are the major cause of device-associated infections [14] and are naturally resistant to antimicrobial agents [28]. Using large inoculums (>10^7) of *Staphylococcus aureus* biofilm-forming clinical isolates, we determined herein that there was a reduction of biofilm formation and a sustained killing over at least 1 week in continuous growing cultures *in vitro*.

The function of B-KPro, an artificial cornea, depends on its optical clarity and refraction. By optical bench testing, we determined that covalent modification with HMPEI did not alter B-KPro's shape, clarity, refractive index, or image-forming quality.

We also determined that HMPEI covalently attached to PMMA conferred no additional cell cytotoxicity or abnormal morphological changes on immortalized human corneal epithelial cells (HCLE), compared to those observed with control PMMA. There were no observable untoward effects on epithelial cell attachment, stratification, differentiation, or proliferation, as compared to PMMA itself. Despite the inherent limitations of 2-D tissue culture models, particularly in the study of 3-D materials, we believe it served as useful screen for cytotoxic effects of comparative materials with similar physical properties. The results reported herein support previous reports of lack of mammalian cell toxicity with monkey kidney cells [9].

In multiple eye compartments in the rabbit *in vivo*, there was no more host tissue reactivity or inflammation observed with HMPEI-bound materials, as compared to the controls, seen by clinical assessment, histopathologic examination, and by SEM. In fact, both in the intrastromal-anterior chamber model and in the B-KPro model, the clinical tissue reactivity (corneal swelling, neovascularization) appeared less by the first week post-operatively with HMPEI-PMMA materials than with the control PMMA materials. By histopathologic examination and by SEM, HMPEI-coated materials showed virtually no more inflammation and more continuous cellular coatings without conspicuous debris than the parent materials.

The B-KPro front plate is composed of PMMA that normally inhibits epithelial overgrowth in both humans and rabbits. Interestingly, we witnessed epithelial overgrowth on HMPEI-coated B-KPro not seen on uncoated PMMA B-KPro. Epithelial overgrowth may obscure vision, however, and is generally undesirable. Yet, epithelial overgrowth might prevent infection and inflammation, and thus may be of potential value particularly in resource-poor areas of the world; it warrants further investigation.

The results of the *in vivo* biocompatibility evaluations conducted in this work are further strengthened by the fact that the rabbit eye is generally more sensitive than the human eye. The rabbit cornea is thinner with a steeper curvature and it is more susceptible to evaporative damage because of a slower blink frequency than a human eye. It also has a heightened tissue response to seemingly minor surgical procedures, foreign materials, drugs, or chemicals. Another factor supporting our findings is that topical corticosteroids were given only for a few days postoperatively; standard clinical postoperative regimens might have masked inflammation in our rabbit experiments. In addition, the rabbit eye readily extrudes foreign material, limiting

long-term studies beyond a few months. It, therefore, seems reasonable to recommend pilot studies in humans.

CONCLUSIONS:

An antimicrobial coating, HMPEI covalently attached to B-KPro materials, has been shown to confer inhibitory effects on biofilm formation by *S. aureus*. HMPEI confers no additional toxicity or reactivity compared to the parent material *in vitro* or *in vivo* in enucleated eyeballs in the adjacent corneal stroma, anterior chamber, or iris. This antimicrobial coating now warrants pilot investigation in human sites that may be easily observable and where the prosthetic material is easily removed and/or exchanged.

References:

1. Baker AS, Schein OD. Ocular infections. *In* Infections Associated with Indwelling Medical Devices. Eds AL Bisno, FA Waldvogel. ASM Press. Washington, D.C. (1989), pp. 75-92.

2. Behlau I, Gilmore MS. Microbial biofilms in ophthalmology and infectious diseases. Arch.Ophthalmol. **126** (2008), 1572-1581.

3. Harissi-Dagher M, Khan BF, Schaumberg DA, Dohlman CH. Importance of nutrition to corneal grafts when used as a carrier of the Boston Keratoprosthesis. Cornea. **26** (2007), 564-568.

4. Dohlman CH, Dudenhoefer EJ, Khan BF, Morneault S. Protection of the ocular surface after keratoprosthesis surgery: the role of soft contact lenses. Clao J. **28** (2002), 72-74

5. Durand ML, Dohlman CH. Successful prevention of bacterial endophthalmitis in eyes with the Boston keratoprosthesis. Cornea. **28** (2009), 896-901

6. Dohlman CH, Harissi-Dagher M, Khan BF, Sippel K, Aquavella JV, Graney JM. Introduction to the use of the Boston keratoprosthesis. Expert Rev Ophthalmol. **1** (2006), 41-48.

7. Bennett-Guerrero E, Pappas TN, Walter A. Koltun WA, Fleshman JW, Lin M , et al for the SWIPE 2 Trial Group*. Gentamicin-collagen sponge for infection prophylaxis in colorectal surgery. N Engl J Med. **363** (2010), 1038-1049.

8. Scott RD II. The direct cost medical costs of healthcare-associated infections in U.S. hospitals and the benefits of prevention. CDC (2009); www.cdc.gov/ncidod/dhqp/pdf/Scott_CostPaper.pdf

9. Milovic NM, Wang J, Lewis K, Klibanov AM. Immobilized *N*-alkylated polyethylenimine avidly kills bacteria by rupturing cell membranes with no resistance developed. Biotechnol Bioeng. **90** (2005), 715-722.

10. Lin J, Tiller JC, Lee SB, Lewis K, Klibanov AM. Insights into bactericidal action of surface-attached poly (vinyl-*N*-hexylpyridium) chains. Biotechnol Lett. **24** (2002), 801-805.

11. Lin J, Qui S, Lewis K, Klibanov AM. Mechanism of bactericidal and fungicidal activities of textiles covalently modified with alkylated polyethylenimine. Biotechnol Bioeng **83** (2003), 168-172.

12. Haldar J, An D, Alvarex de Cienfuegos L, Chen J, Klibanov AM. Polymeric coatings that inactivate both influenza virus and pathogenic bacteria. Proc Natl Acad. Sci USA. **103** (2006), 17667-17671.

13. Lowy FD. *Staphylococcus aureus* infections. N Engl J of Med. **339** (1998), 520-532.

14. Darouiche RO. Treatment of infections associated with surgical implants. N Engl J Med. **350** (2004), 1422-1429.

15. Ciolino JB, Hoare TR, Iwata NG, Behlau I, Dohlman CH, Langer R, Kohane DS. Drug-eluting contact lens. IOVS. **50** (2009), 3346-3352.

16. Jefferson KK, Cramton SE, Götz, F Pier GB. Identification of a 5-nucleotide sequence that controls expression of the *ica* locus in *Staphylococcus aureus* and characterization of the DNA-binding properties

of IcaR. Molec Microbiol. **48** (2003), 889-899.

17. Schlievert, P. M. Blomster, D. A. (1983) Production of staphylococcal pyrogenic exotoxin type C: influence of physical and chemical factors. J Infect. Dis. **147** (2003), 236–242.
18. National Committee for Clinical Laboratory Standards. ApprovedStandard M7–A7. Methods for Dilution Antimicrobial Susceptibility

21. Christensen GD, Simpson WA, Younger JJ, Baddour LM, Barrett FF, Melton DM, Beachey EH. 1985. Adherence of coagulase-negative staphylococci to plastic tissue culture plates: a quantitative model for the adherence of staphylococci to medical devices. J Clin Microbiol. **22** (1985), 996–1006.

22. Argueso P, Tisdale A, Spurr-Michaud S, Sumiyoshi M, Gipson IK. Mucin characteristics of human corneal-limbal epithelial cells that exclude the rose bengal anionic dye. Invest Ophthalmol Vis Sci. **47** (2006), 113-119.

23. Harissi-Dagher M, Beyer J, Dohlman CH. The role of soft contact lenses as an adjunct to the Boston keratoprosthesis. Int Ophthalmol Clin. **48** (2008), 43-51.
24. Shimizu K, Kobayakawa S, Tsuji A, Tochikubo T. Biofilm formation on hydrophilic intraocular lens material. Curr Eye Res. **31** (2006), 989-997.

24B. Lewis K, Klibanov AM. Surpassing Nature: rational design of sterile-surface materials. Trends Biotechnol. **23** (2005), 343-348.

25. Heimer SR, Yamada A, Russel H, Gilmore MS. Response of corneal epithelial cells to *Staphylococcus aureus*. Virulence. **1** (2010), 223-235.

26. Vancha AR, Govindaraju S, Parsa KVL, Jasti M, Gonzalez-Garcia M, Ballestero RP. Use of polyethyleneimine polymer in cell culture as attachment factor and lipofection enhancer. BMC Biotechnol. **4** (2004), ????.

27. Khalifa YM, Davis D, Mamalis N, Moshirfar M. **Epithelial growth over the optic** surface of the type 1 Boston Keratoprosthesis: histopathology and implications for biointegration Clin Opthalmol. 4 (2010), 1069-1071.

28. Williams DF. On the mechanisms of biocompatibility. Biomaterials. **29** (2008), 2941-2953.

29. Williams DF. On the nature of biomaterials. Biomaterials. **30** (2009), 5897-5909.

30. Costerton JW, Stewart PS, Greenberg EP. Bacterial biofilms: a common cause of persistent infections. Science. **284** (1999), 1318-1322.

31. Booth MC, Hatter KL, Miller D, et al. Molecular epidemiology of *Staphylococcus aureus* and *Enterococcus faecalis* in endophthalmitis. Infect Immun. **66** (1998), 356-360.

32. Behlau I, Leonard EM, Heimer SH, Martin JN, DohlmanCH, Gilmore MS. Characterization of keratitis-associated *Staphylococcus aureus* infections from the Boston area. Ocular Microbiol Immunol Group (2008) Abstract 14. http://eyemicrobiology.upmc.com/2008 Abstracts/2008 OMIG Abstract 14.html

33. Behlau I, Heimer SR, Leonard EM, Martin JN, Dohlman CH, Gilmore MS. *Staphylococcus aureus*-associated keratitis: phenotypic and genotypic characterization. ARVO (2009) 5113-D1059.

34. Klibanov AM. Permanently microbicidal materials coatings. J. Mater. Chem. **17** (2007), 2479-2482.